A GIS-Based Flood Forecasting Model for the Duffins Creek Watershed, Ontario

by

C. Darren Sutton

A Research Paper

Presented to Ryerson University

in partial fulfillment of the requirements for the degree of

Master of Spatial Analysis

A joint program with the University of Toronto

Toronto, Ontario, Canada

Author's Declaration

I hereby declare that I am the sole author of this Research Paper

I authorize Ryerson University to lend this Research Paper to other institutions or individuals for the purposes of scholarly research.

_____

C. Darren Sutton

Abstract

Organizations such as the Toronto and Region Conservation Authority (TRCA) could benefit from a flood forecasting method that uses GIS tools and spatial data because they have already invested in GIS software. This research project utilized a 30-metre resolution Digital Elevation Model (DEM), shapefiles of land cover and soil type, and a Landsat 7 Enhanced Thematic Mapper (ETM+) satellite image to delineate hydrological response units. Snowpack depths were simulated using data from The Weather Network and modelling using the Guelph All-Weather Storm Event Runoff (GAWSER) equations. The Curve Number Method was used to predict peak discharge and time to peak discharge.

Snowpack depth was overestimated in some cases, which is likely due to error in snowfall simulations and underestimation of the melt factor. A systematic error, which was caused by averaging of rainfall inputs was corrected for by reducing simulated peak discharge by a factor of 10. The model is most adept at simulating peak discharge for a 71.6 mm rainfall event. For smaller events, a multiplier was introduced to improve the model's performance. Snowpacks did not have a significant impact on peak discharge although runoff increased slightly. Underestimation of time to peak for some simulations is due to the effects of tillage and error in estimation of channel flow velocity. Despite some errors, a workable model was obtained that could be useful to organizations like the TRCA.

Acknowledgements

I would like to thank my graduate faculty advisor, Dr. Wayne Forsythe for his valuable advice and assistance during the course of this research and throughout my studies as a Master of Spatial Analysis student. I would also like to thank Dr. Shuguang Wang, the program's current director and outgoing director Dr. Marie Truelove. I am particularly indebted to Dr. Truelove for arranging a practicum position with the Toronto and Region Conservation Authority (TRCA). My experience at the TRCA was instrumental to the completion of this research. Dr. James Li (Civil Engineering) provided valuable advice on a systematic error encountered during model validation. Additionally, my MSA classmates provided advice and encouragement on many occasions.

During my practicum with the TRCA I was supplied with data, advice and assistance which were all helpful towards the completion of this research. I would like to thank the following individuals:

Hendrik Amo, *Geomatics Specialist, Information Systems/Information Technologies* who also supervised my practicum;

Donald Haley, *Water Resources Engineer*, and;

Jason Tam, *Geomatics Specialist, Information Systems/Information Technologies*

TRCA data was used for this research in accordance with a Memorandum of Understanding signed by both Ryerson University and the TRCA. Digital

Orthophotographs were used by permission via a Data Release Agreement signed by the author and a Ryerson University library representative.

Table of Contents

List of Tables

List of Figures

List of Acronyms

DEM	Digital Elevation Model
DML	Dynamic Modelling Language
ETM+	Enhanced Thematic Mapper +
FFOR	Flood Forecasting Model
GAWSER	Guelph All-Weather Storm Event Runoff
GCM	General Circulation Model
GIBSI	Gestion Intégrée des Bassins versants à l'aide d'un Système Informatisé
GIS	Geographic Information System
HEC	Hydrologic Engineering Centre
HMS	Hydrological Modelling System
LAI	Leaf Area Index
MMS	Modular Modelling System
NAD	North American Datum
NDVI	Normalized Difference Vegetation Index
OMNR	Ontario Ministry of Natural Resources
OTTHYMO	Ottawa Hydrologic Model
RMSE	Root Mean Square Error
SWMM	Storm Water Management Model
TIN	Triangular Irregular Network
TOPMODEL	Topography Based Hydrological Model
TRCA	Toronto and Region Conservation Authority
WMS	Watershed Modelling System

Chapter 1: Introduction

Flood forecasting models are tools that can be used as warning systems for activities on floodplains. Models can be classified as stand-alone or Geographic Information System (GIS) integrated. Stand-alone models are usually custom software packages that may be designed for specific platforms. Examples include the Watershed Modelling System (WMS), the Gestion Intégrée des Bassins versants à l'aide d'un Système Informatisé (GIBSI), the Modular Modelling System (MMS), PCRaster, and the Topography Based Hydrological Model (TOPMODEL). Some stand-alone models have mapping or GIS modules, but tend to lack the intuitive visualization and spatial analysis functions that are available in standard GIS software (Al-Sabhan et al., 2002). These tools, along with the ability to process large amounts of spatial data, are both characteristics of GIS that make it suitable for use in flood forecasting.

The Toronto and Region Conservation Authority (TRCA) is a municipal organization that protects and monitors the natural environment in the Greater Toronto Area. The TRCA's jurisdiction covers nine watersheds located in the City of Toronto, the Regional Municipalities of Durham, Peel, and York, as well as Dufferin, and Simcoe Counties. Part of its mandate includes the administration of a flood forecasting and warning program designed to monitor watershed conditions and issue flood messages to municipalities (TRCA, 2003). The Duffins Creek Watershed, which serves as the study area for this project, is located in the TRCA's jurisdiction north of Ajax, Ontario (Figure 1.1).

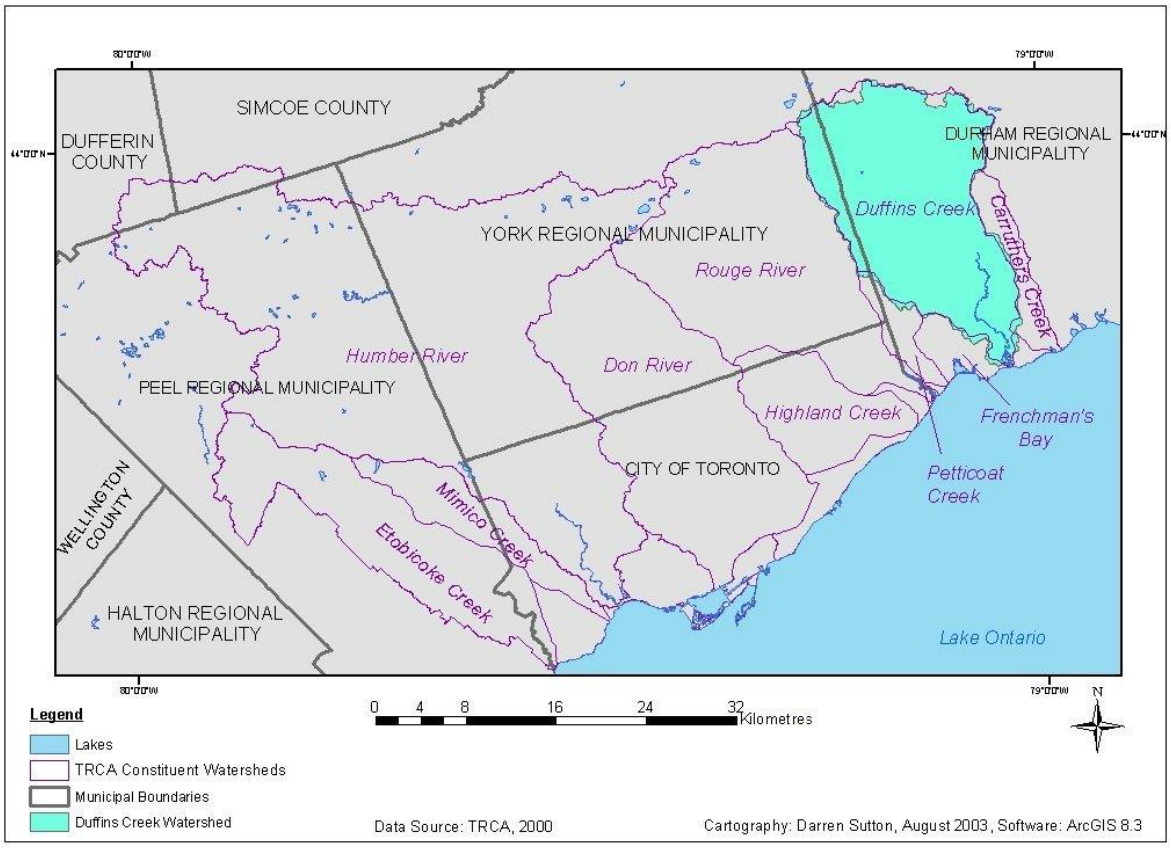

Figure 1.1: Location of the Duffins Creek Watershed Within the Jurisdiction of the Toronto and Region Conservation Authority

The TRCA has recently started to use ArcView 3.2 (ESRI, 2002) to generate hydrological data for input into a flood-forecasting model. Previously, they used the Visual Ottawa Hydrologic Model (OTTHYMO) to generate forecasts. This model simulates flood discharge based on unit hydrograph theory (Watercom Engineering, 2002). A hydrograph represents a time series of river discharge during a flood. A unit hydrograph is defined as the basin outflow resulting from 2.52 centimetres (or one inch) of direct runoff generated uniformly over the drainage area at a uniform rainfall rate during a specified period of rainfall duration (Sherman, 1932). This model is effective but

the use of unit hydrograph theory involves several assumptions that can limit its application (Bedient and Huber, 2002). These are:

1) Rainfall excesses of equal duration are assumed to produce hydrographs with equivalent time bases regardless of the intensity of rain.
2) Direct runoff volume for a storm of a given duration is assumed to be directly proportional to rainfall excess volume. Thus, twice the rainfall produces a doubling of hydrograph volume.
3) The time distribution of direct runoff is assumed independent of antecedent precipitation.
4) Rainfall distribution is assumed to be the same for all storms of equal duration, both spatially and temporally.

Given these limitations, forecasting based on a physical model of the watershed may be a more versatile solution. Such a model is feasible when GIS is used in combination with the Curve Number Method. This project uses a GIS-based method to generate flood forecasts. It is meant to be a proof of concept, which the TRCA can use to evaluate the feasibility of switching to GIS-based forecasting as opposed to using unit hydrograph theory. Since the TRCA has already made a significant investment in GIS, the transition between their current flood forecasting software and GIS should not be a barrier.

Developing models within a GIS as opposed to developing a separate hydrological model that works in combination with a GIS eliminates several problems associated with transferring data between GIS and other software. Specifically, these are the lack of a common interface, differences in data models, and cumbersome data exchange (Al-Sabhan et al., 2002). Models developed entirely within a GIS, referred to as tightly-coupled models, have been criticized because they cannot easily support complex custom applications and require the development of a user interface (Karimi and Houston, 1997; Al-Sabhan et al., 2002). These problems can be solved or reduced by

performing calculations or solving equations in a spreadsheet software package such as Microsoft Excel or Corel Quattro-Pro. This necessitates exporting data out of the GIS, but spatial data need only be stored in some tabular format for use in a spreadsheet (.dbf or delimited text) making them easily transferable.

1.1 Flood Forecasting Theory

Flood forecasts are produced by simulating stream discharge for a series of time steps. During a flood, discharge rises in proportion to the volume of runoff from the watershed. Runoff is assumed to originate as surface detention, which is defined as that part of rain that does not immediately infiltrate into the soil. A portion of the surface detention becomes runoff after local depressions have been filled. The depth of water at which depressions are filled is referred to as the filling depth. The maximum surface detention storage (S_{max}) is defined as:

$$S_{max} = \int_0^{s_{max}} s\, \ell\,(s)\, ds \qquad (1)$$

where s is the filling depth, s_{max} is the maximum filling depth, and ℓ is the area of the depression expressed as a fraction of the whole catchment. The term ℓ (s) is written as such because ℓ is a function of the filling depth s (Hall, 1981).

S_{max} is a significant term because it denotes the maximum amount of water that can accumulate as surface detention and thus represents a limit on runoff. The rate of

infiltration and S_{max} both depend on soil type and soil wetness. Much of the available knowledge on infiltration rates derives from experiments performed in controlled environments (Hall, 1981). A satisfactory theory describing the variation of infiltration in natural environments is unavailable.

As an alternative, empirical formulae have been developed that describe the rainfall-runoff response of the watershed. Use of these methods usually involves dividing the watershed into units that produce approximately the same volume of runoff per unit area per input of precipitation. These units are called hydrological response units (Mockus, 1964).

1.1.1 The Curve Number Method

The Curve Number Method defines hydrological response units based on soil type, land use, and ground cover. Soils are divided into four principal groups (Mockus, 1964);

A. Soils with low runoff potential. Soils having high infiltration rates even when thoroughly wetted and consisting chiefly of deep, well drained to excessively well-drained sands or gravels.

B. Soils having moderate infiltration rates even when thoroughly wetted and consisting chiefly of moderately deep to deep, moderately well drained to well drained soils with moderately fine to moderately coarse textures.

C. Soils having slow infiltration rates even when thoroughly wetted and consisting chiefly of soils with a layer that impedes downward movement of water, or soils with moderately fine to fine textures.

D. Soils with high runoff potential. Soils having very slow infiltration rates even when thoroughly wetted and consisting chiefly of clay soils with a high swelling potential, soils with a permanent high water table, soils with a claypan or clay layer at or near the surface, and shallow soils over nearly impervious material.

A useful definition of curve numbers is shown in Table 1.1. For each hydrological unit, S_{max} is defined as a function of the curve number (CN):

$$S_{max} = 25400/CN-254 \quad (2)$$

Effective runoff (W_{eff}) is calculated using S_{max} and precipitation depth (P) where all terms are expressed in mm:

$$W_{eff} = (P - 0.2S_{max})^2/(P + 0.8\ S_{max}) \quad (3)$$

The volume of runoff (R) released from a given hydrological unit is determined by:

$$R = A\ W_{eff} \quad (4)$$

where A is the area of the hydrological unit.

1.1.2 Travel Time

Runoff travels through the watershed in three principal phases; sheet flow, shallow concentrated flow, and channel flow. Runoff begins as sheet flow, which is

Table 1.1: Curve Number Definitions (Source: Chow et al., 1988)

Description of Land Use	**Hydrologic Soil Group**			
	A	**B**	**C**	**D**
Paved parking lots, roofs, driveways	98	98	98	98
Streets and Roads:				
Paved with curbs and storm sewers	98	98	98	98
Gravel	76	85	89	91
Dirt	72	82	87	89
Cultivated (Agricultural Crop) Land*:				
Without conservation treatment (no terraces)	72	81	88	91
With conservation treatment (terraces, contours)	62	71	78	81
Pasture or Range Land:				
Poor (<50% ground cover or heavily grazed)	68	79	86	89
Good (50-75% ground cover; not heavily grazed)	39	61	74	80
Meadow (grass, no grazing, mowed for hay)	30	58	71	78
Brush (good, >75% ground cover)	30	48	65	73
Woods and Forests:				
Poor (small trees/brush destroyed by over-grazing or burning)	45	66	77	83
Fair (grazing but not burned; some brush)	36	60	73	79
Good (no grazing; brush covers ground)	30	55	70	77
Open Spaces (lawns, parks, golf courses, cemeteries, etc.):				
Fair (grass covers 50-75% of area)	49	69	79	84
Good (grass covers >75% of area)	39	61	74	80
Commercial and Business Districts (85% impervious)	89	92	94	95
Industrial Districts (72% impervious)	81	88	91	93
Residential Areas:				
1/8 Acre lots, about 65% impervious	77	85	90	92
1/4 Acre lots, about 38% impervious	61	75	83	87
1/2 Acre lots, about 25% impervious	54	70	80	85
1 Acre lots, about 20% impervious	51	68	79	84

flow over a plane surface with a depth of approximately 0.03 metres. Sheet flow persists for a maximum of 92 metres, after which shallow concentrated flow begins (Eaglin, 1996).

The travel time (TT) of sheet flow (hours) is determined by:

$$TT = 0.007(nL)^{0.8}/(P2^{0.5}S^{0.4}) \quad (5)$$

where n is Manning's Roughness Coefficient, L is the length of flow (feet), P2 is the depth of a 2-year, 24-hour rainfall (inches) and S is slope (Overton and Meadows, 1976). The parameter n depends on the type of terrain where sheet flow occurs (Table 1.2).

Table 1.2: n Values for Sheet Flow (Source: modified after Eaglin, 1996)

Surface Description	n
Smooth Surfaces	0.011
Fallow (No Residue)	0.05
Cultivated Soils, Residue Cover <= 20%	0.06
Cultivated Soils, Residue Cover > 20%	0.17
Short Grass Prairie	0.15
Dense Grass	0.24
Bermuda Grass	0.041
Range (Natural)	0.13
Woods, Light Underbrush	0.4
Woods, Dense Underbrush	0.8

Shallow concentrated flow usually persists from the point at which sheet flow ends until the runoff enters a river channel. The average velocity of shallow concentrated flow is a function of the watercourse slope (Figure 1.2). Travel time (hours) of shallow concentrated flow is calculated using:

$$TT = L/(3600V) \quad (6)$$

where L is the length of flow and V is the average velocity of flow. Shallow concentrated flow can be diverted by tillage so that it might not always run directly down slope (Eaglin, 1996). This may result in longer travel times than predicted.

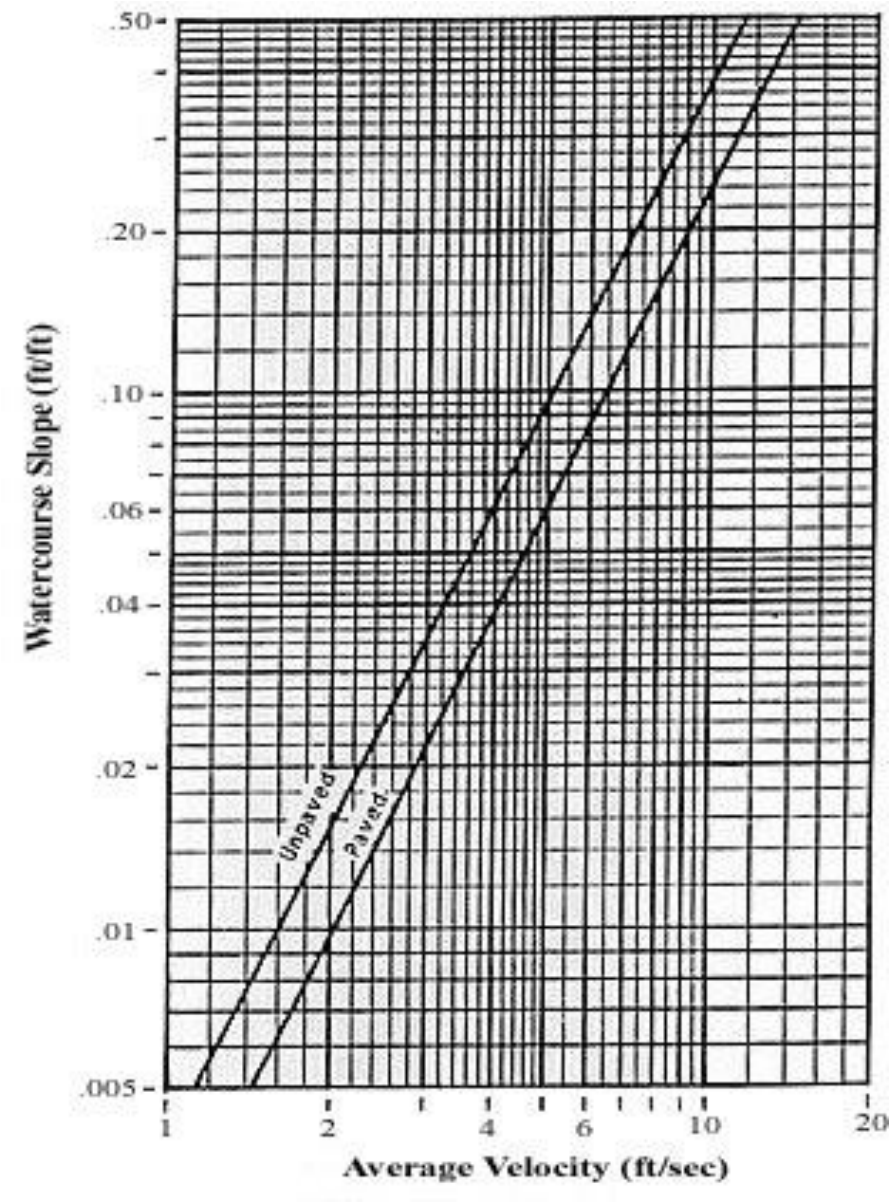

Figure 1.2: Average Velocity of Shallow Concentrated Flow
(Source: Blevins, 2003)

The velocity of open channel flow (m/s) is determined by:

$$V = 1/nR^{2/3}S^{1/2} \quad (7)$$

where n is Manning's Roughness Coefficient, R is the Hydraulic Radius of the channel and S is slope (Eaglin, 1996). Selecting the appropriate value for n depends on the characteristics of the stream channel (Table 1.3).

Table 1.3: n Values for Channel Flow (Source: Edwards, 1998)

Type of Stream	n
Clean and Straight	0.03
Major River	0.035
Sluggish With Deep Pools	0.04

The Hydraulic Radius of a natural stream channel is defined as the ratio of the cross-sectional area of the stream to the wetted perimeter. The wetted perimeter is defined as the total length of the channel bed beneath the river, measured across the river (Brennan and Smith, 1997). Travel time for open channel flow is determined using the same equation as for shallow concentrated flow.

1.1.3 Snow Infiltration Modelling

In the presence of snow, the retention and melt of the pack must be considered before the Curve Number Method is applied. There are several snowmelt/accumulation models, which tend to be complex and have numerous input parameters (i.e. Kutchment and Gelfan, 1996, Pomeroy et al., 1998). An alternative is the Guelph All-Weather Storm

Event Runoff (GAWSER) snow/rain routine, consisting of a series of simple equations that estimate available runoff from a snowpack (Hinckley Jr., 1996). The inputs to this model are the initial snowpack depth, air temperature, a melt factor, and a refreeze factor.

Melt and refreeze factors are dependent on the location, cover, exposure to solar radiation, time of year, and meteorological conditions (Doherty and Switzer, 2000). The Flood Forecasting (FFOR) spreadsheet model, which was prepared by the Environmental Water Resources Group Ltd., estimates these two parameters as a basic function of the month of the year (Doherty and Switzer, 2000). Other authors have used long-term gauge records (Kutchment and Gelfan, 1996), a pre-determined function of antecedent temperature (Daly et al., 2000), or averages of literature values (Semàdeni-Davies, 1997).

In general, using melt and refreeze factors is not recognized as the most accurate method for estimating snow melt because the scatter of points around the best-fit line tends to be great. However, for rapid, approximate predictions of melt or in the absence of energy balance data, they yield usable results (Dunne and Leopold, 1978).

The FFOR model estimates melt and refreeze factors as a function of the month of the year for the Halton Region, Ontario (Table 1.4).

Table 1.4: Melt/Refreeze Factors for Halton Region, Ontario (Source: Doherty and Switzer, 2000)

Month	KM/KF
January	2.7
February	3.7
March	5.1
April	6.8
May	8.0
June	10.0
July	8.0
August	6.8
September	5.1
October	3.7
November	2.7
December	2.1

The GAWSER equations fall into five categories (Hinckley Jr., 1996).

1) New Snow Additions

$$Depth_f = Depth_0 + Snow \quad (8)$$

$$SWC_f = SWC_0 + SWC_n \quad (9)$$

$$SWC_n = 0.1*Depth + Snow \quad (10)$$

$$\rho = SWC_f / Depth_f \quad (11)$$

$$P = 1 - \rho/0.92 \quad (12)$$

where Depth = snowpack depth (mm), Snow = new snow (mm), SWC = solid water content of the snowpack (mm), ρ = relative dry density of the snowpack (g/cm^3) and P = porosity of the snowpack (vol/vol).

2) Snowmelt

$$Melt = KM*(DT/24)*(T) \text{ for } T>0 \quad (13)$$

$$SWC_f = SWC_0 - Melt \quad (14)$$

$$Depth_f = SWC_f / \rho \quad (15)$$

$$LWC_f = LWC_0 + Melt + Rain \quad (16)$$

where Melt = potential snowmelt (mm) and is equal to 0 when T is less than 0°C, T = air temperature (°C), KM = melt factor (mm/d/°C), DT = time interval (hours) and Rain = rainfall (mm).

3) Refreeze of Snowpack Liquid Water

$$Refrz = KF*(DT/24)*(0-T) \text{ for } T<0 \quad (17)$$

$$LWC_f = LWC_0 - Refrz \quad (18)$$

$$SWC_f = SWC_0 + Refrz \quad (19)$$

where Refrz = refrozen water (mm) and is equal to 0 when T is greater than 0°C and KF = refreeze factor (mm/d/°C). It is assumed that KM = KF which is the initial assumption of the FFOR model.

4) Snowpack Compaction

$$\rho_{new} = (\rho*0.35)/(\rho+\{0.35 - \rho\}^{\{-DT/KC\}}) \quad (20)$$

$$KC = B^{(-A*T)} \quad (21)$$

$$\rho_f = \rho_0 \text{ for } \rho_{new} >= 0.35 \quad (22)$$

$$\rho_f = \rho_{new} \text{ for } \rho_{new} < 0.35 \quad (23)$$

where KC = Compaction Time Constant (hours), A = 1/T and B = time since snowfall (hours).

5) Release of Snowpack Liquid Water

$$Cap = P^* 0.07^*Depth \quad (24)$$

$$W = LWC_i - Cap \text{ for } LWC_i > Cap \quad (25)$$

$$W = 0 \text{ for } LWC_i <= Cap \quad (26)$$

$$LWC_f = Cap \quad (27)$$

where Cap = liquid water capacity of snow pack (mm) and W = runoff (mm).

1.2 Study Area

The Duffins Creek Watershed (Figure 1.3) covers a 283 km^2 area incorporating a large portion of the Town of Pickering and small portions of Ajax, Uxbridge, Whitchurch-Stouffville and Markham. The headwaters are located in the Oak Ridges Moraine and the outlet empties into Lake Ontario. The Town of Ajax is located in the southeast corner of the watershed. Major tributaries include Stouffville Creek, Wixon Creek, Whitevale Creek, Major Creek, Urfe Creek, Brougham Creek, Ganatsekiagon Creek, and Mitchel Creek. Major sedimentary units include the Oak Ridges Moraine, the Halton Till Plain, the Lake Iroquois Shoreline, and the Lake Iroquois Plain. The northern and middle sections of the watershed are primarily rural where the dominant land use is agriculture. The southern section along the Lake Ontario shoreline is comprised primarily urban and suburban land (TRCA, 2002b).

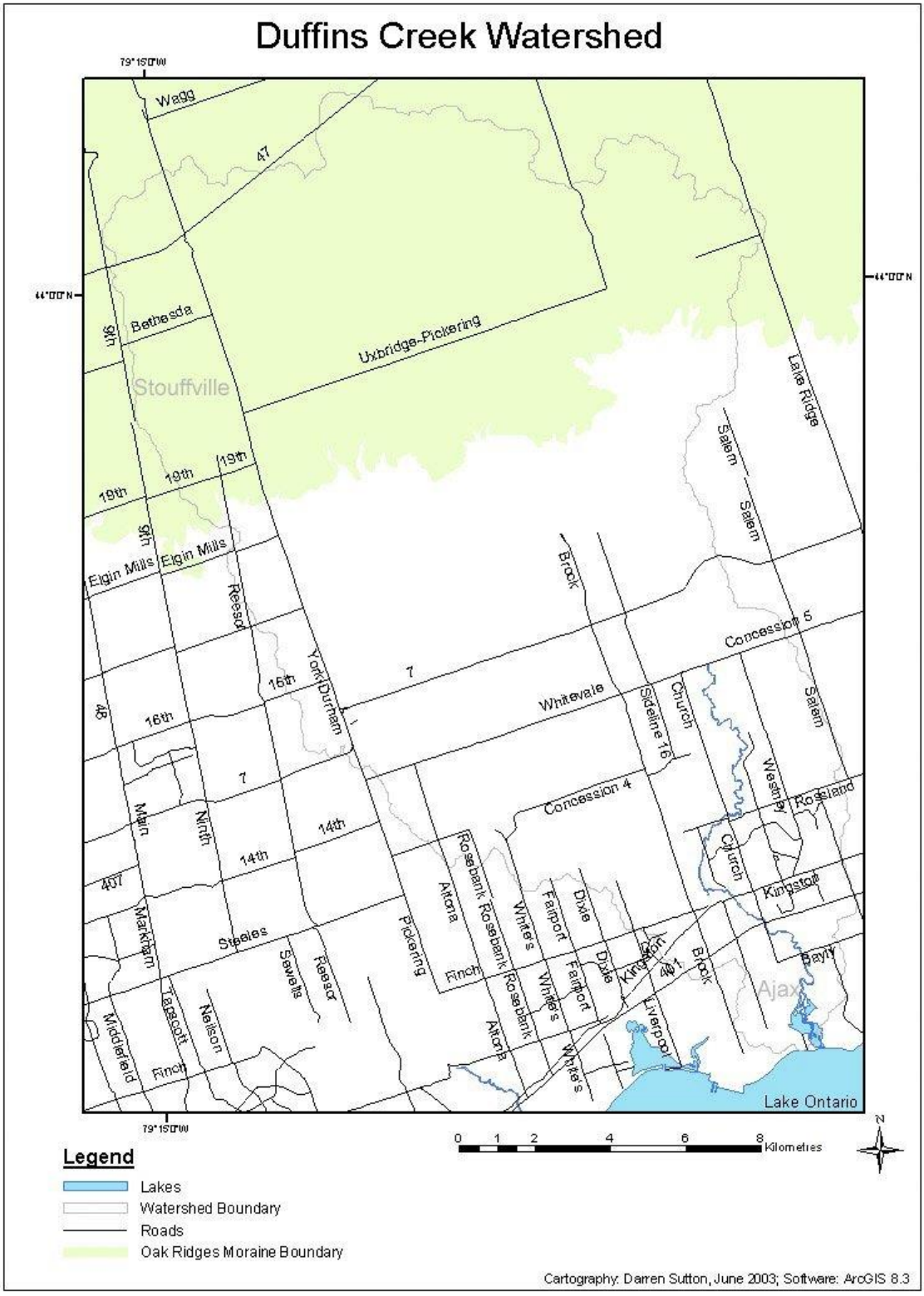

Figure 1.3: The Study Area

1.2.1 Surficial Geology

Loam and Sandy Loam cover most of the watershed area (Figure 1.4 and Table 1.5). Silt Loam is also present but is scarce. Patches of Clay are found along the western reaches while Clay Loams are concentrated in the urbanized south. Small patches of organic soils and sand also occur, the latter only in the north. Fluvial sediments, which are found in and around stream channels, have mixed grain sizes.

Table 1.5: Surficial Geology in the Duffins Creek Watershed
(Source: TRCA, 2000)

Surficial Geology	Total Area (km^2)	Percent of Total Watershed Area
Clay	24.9	8.8
Clay Loam	11.0	3.9
Loam	122.3	43.2
Organic	3.9	1.4
Sand	4.2	1.5
Sandy Loam	90.3	31.9
Silt Loam	0.8	0.003
Variable	25.4	9.0

Most Loams in the watershed fall into Hydrological Soil Group B. Hence, this is the primary soil group found in the study area. Clays fall into Group D while fluvial sediments, Clay Loams, and Silt Loams are classified as Group C. Some Sandy Loams and sands in the northern part of the watershed fall into Group A.

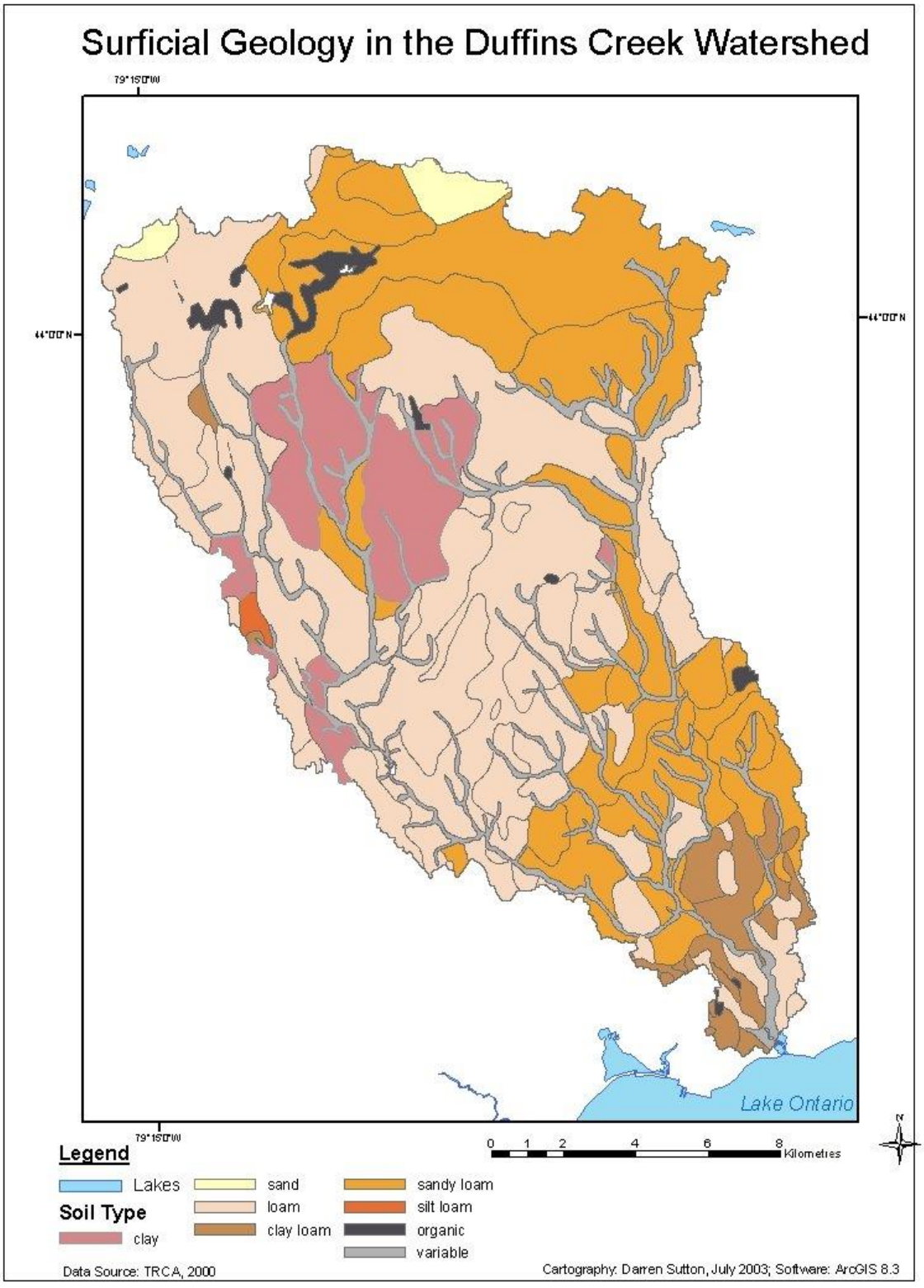

Figure 1.4: Surficial Geology

1.2.2 Land Cover

The majority of land in the watershed is used for agriculture amounting to an area of approximately 172 km^2 or 61% of the total (Table 1.6 and Figure 1.5). Some of this land has been reserved solely for agriculture by the York and Durham Regional Municipalities (TRCA, 2002b). Also included is a 51 km^2 section classified as Federal Airport Lands, the vast majority of which is cropland. Forest is found along the stream channels and in the northeast. Small patches of meadow are found throughout the watershed, and consist mainly of agricultural land that is not being cultivated or pasture with some open fields. Most of the area being used for urban and urban open space is associated with the Towns of Ajax and Whitchurch-Stouffville. However, some rural estates also exist. Wetlands are found in the north and at the outlet by Ajax.

Table 1.6: Land Cover in the Duffins Creek Watershed (Source: TRCA, 2000)

Land Cover	Total Area (km^2)	Percent of Total Watershed Area
Agricultural Reserve	6.4	2.3
Agricultural/Rural	98.9	35.0
Federal Airport Lands	50.9	18.0
Forest	73.8	26.1
Meadow	25.0	8.8
Urban	19.6	6.9
Urban Open Space	2.6	0.9
Wetland	5.7	2.0

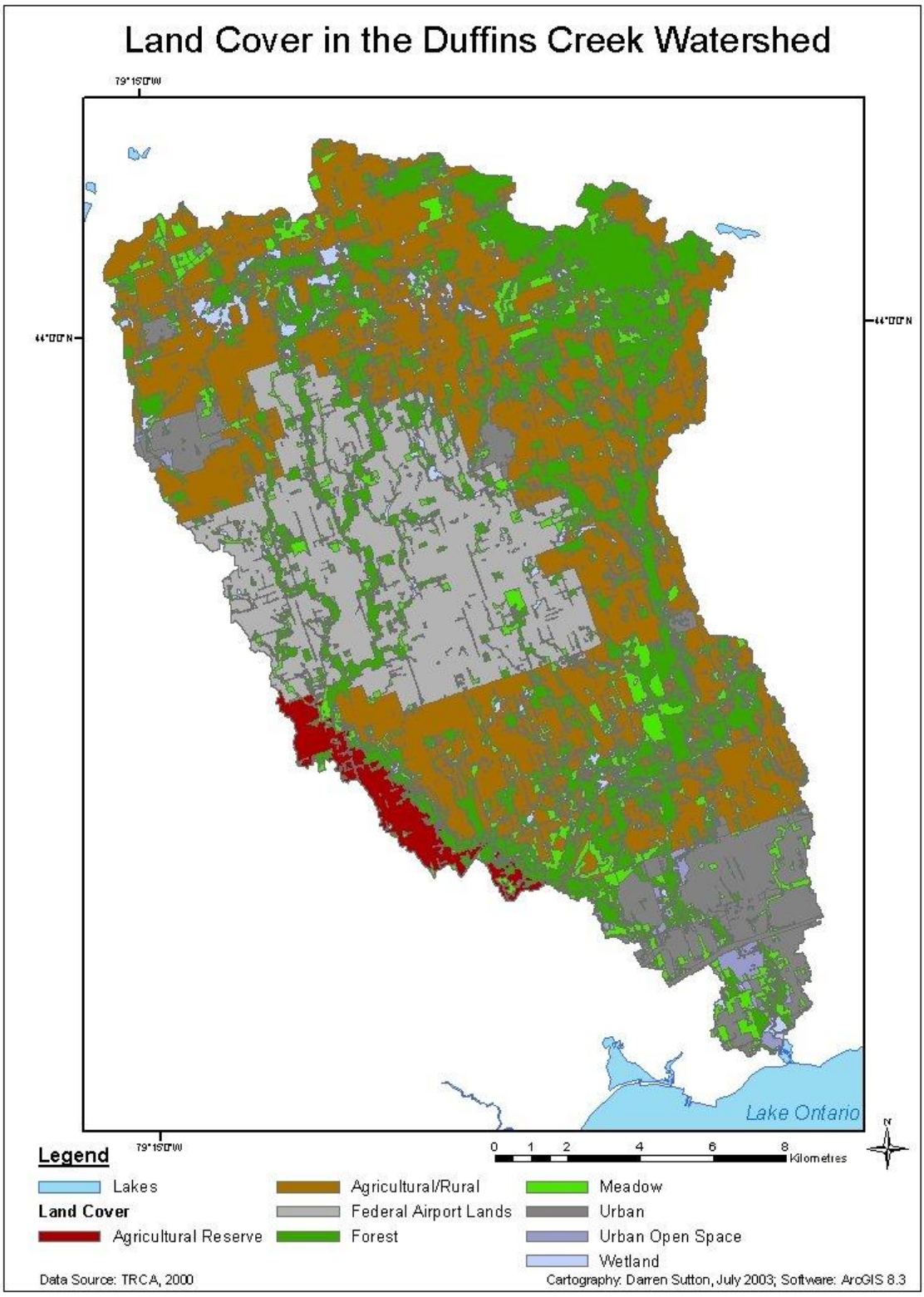

Figure 1.5: Land Cover

1.2.3 Population

Population distribution in the Duffins Creek Watershed must be taken into account when assessing flood risk (Figure 1.6). Cities and towns are generally at greater risk with respect to loss of life, injury and damage to housing because population is higher in urban areas than the surrounding country. Approximately 76000 people reside in the Town of Ajax (Town of Ajax, 2003) making it the most populated municipality in the watershed. The Town of Whitchurch-Stouffville is smaller with approximately 24343 residents (Town of Whitchurch-Stouffville, 2003), but is still a significant population centre.

1.3 The Problem

The use of GIS software has become very common in numerous fields ranging from business to environmental science (ESRI, 2003). GIS tools have become sufficiently sophisticated to solve complex spatial problems, including the mapping and timing of rainfall runoff. GIS software is often used to prepare input data for hydrological models (Al-Sabhan et al., 2002). However, using a separate software package to generate forecasts is a step that could be avoided if spatial data and GIS tools could be used for forecasting. This would allow GIS specialists or non-flood experts with sufficient GIS knowledge to produce forecasts and might also make forecasting more efficient since only one software package would be required.

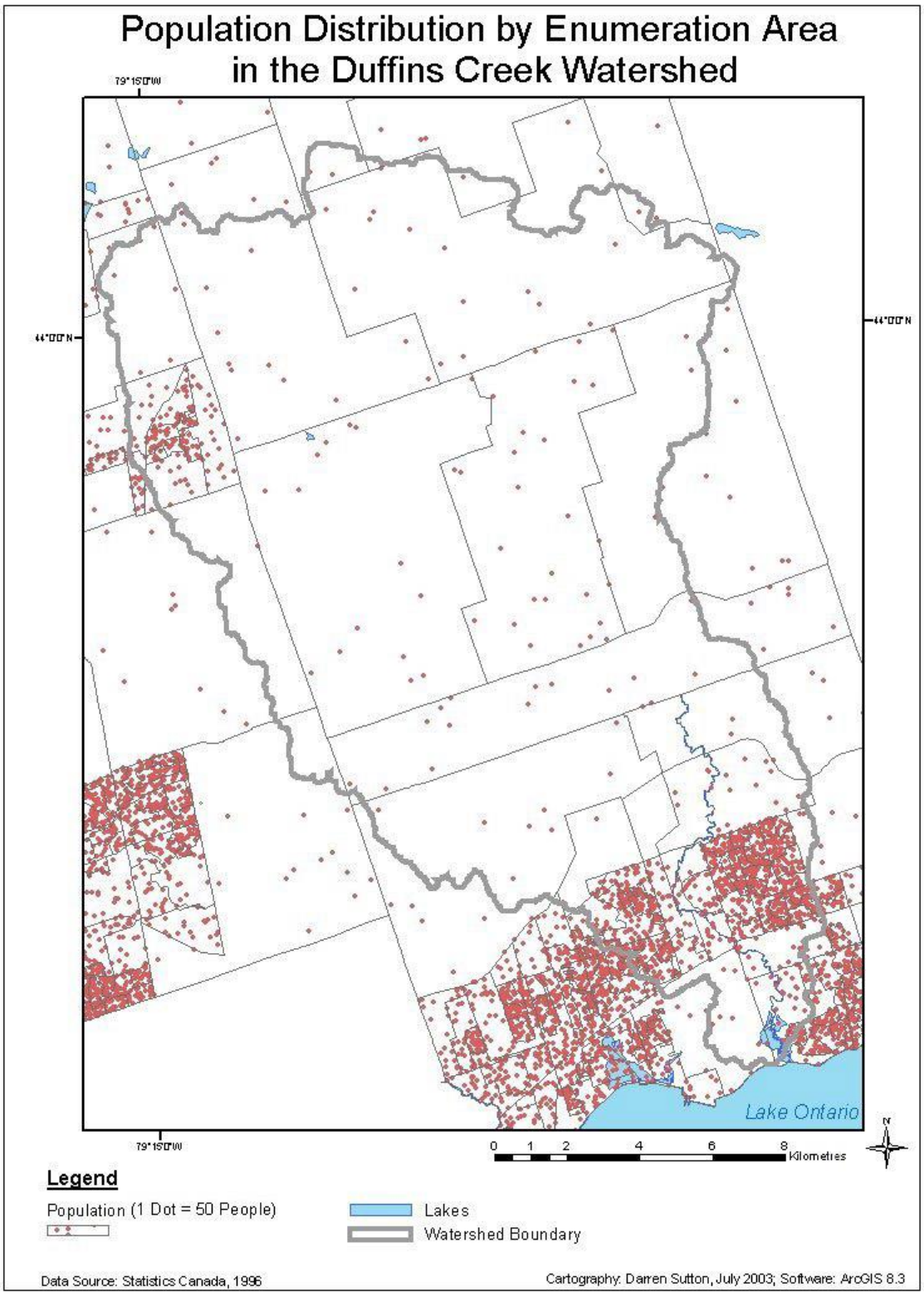

Figure 1.6: Population Distribution

1.3.1 Objectives

A flood-forecasting model will be developed for the Duffins Creek Watershed using GIS software and spatial data. Flood hydrographs created using Visual OTTHYMO (TRCA, 2002a) will be used for verification of the results and calibration. Design storms with 2-year, 5-year, and 10-year recurrence intervals will be used to generate forecasts. The project was undertaken with three objectives in mind:

1) Predict peak hydrograph discharge within 10 m^3/s and time to peak discharge within 1 hour;
2) Emphasize simplicity so that the same methods could be applied to another watershed;
3) Generate flood forecasts for 2-year, 5-year, and 10-year storms and assess risk to anthropogenic developments.

1.3.2 Software

Since ArcView 3.2 is the GIS package that is presently used by the TRCA, it is logical to use it for this project. Additionally, ArcView 3.2 and 8.3 are both extremely popular software packages with an estimated one million+ people using them every day (ESRI, 2003). It should be noted that an extension for ArcView exists that performs several hydrological modelling functions. ArcHydro uses a relatively detailed representation of a watershed's stream networks and drainage basins to produce time series' of flow (ESRI, 2001). It was not available for use in this project and may not have been suitable anyway since it does not take explicit account of soil type or land use.

The United States Army Corps of Engineers Hydrological Engineering Centre (HEC) has created a Hydrological Modelling System (HMS) extension for ArcView 3.2 called HEC-GeoHMS. This extension was used to delineate sub-basins and stream networks in the Duffins Creek watershed. HEC-GeoHMS uses a Digital Elevation Model (DEM) to estimate flow direction and accumulation based on predicted flow between grid cells (water flows to the adjacent grid cell with the lowest elevation). McLin et al. (2001) used it to predict changes in hydrograph peaks following wildfire. Although the overall discharge was overestimated, the time to peak and peak discharge were estimated very accurately. In a more complex procedure, Anderson et al. (2002) integrated HEC-GeoHMS with an atmospheric mesoscale model and reported that their method showed promise.

Chapter 2: Literature Review

2.1 Review of Flood Forecasting Software

Many flood forecasting models exist, some of which are widely used while others have not been widely accepted. A review of commonly referenced models serves to illustrate that a large range of model frameworks and applications exist. Additionally, only a few models have integrated GIS tools (i.e. WMS) or links to GIS software packages (i.e. SWMM), highlighting the relevance of this research.

2.1.1 TOPMODEL

The Topography Based Hydrologic Model (TOPMODEL) bases its predictions on an analysis of catchment topography. It predicts saturation and infiltration excess surface runoff as well as subsurface flow. The model emphasizes simplicity and can be modified to incorporate the user's knowledge and perceptions of the watershed (Beven, 2001). TOPMODEL predictions are based on the topographic index (TI):

$$TI = \ln(a/\tan\beta) \tag{28}$$

where a is the area draining through a point from upslope and β is the local slope angle. The topographic index is estimated from a Digital Elevation Model (DEM) of the watershed. Areas with high index values tend to saturate quicker and are thus more likely to produce runoff. Areas with the same or very similar topographic indices are analogous

to hydrological response units. They are assumed to have essentially the same rainfall-runoff response (Beven, 1997). Two fundamental assumptions are associated with the topographic index method. These are:

1) that the dynamics of the water table can be approximated by uniform subsurface runoff production per unit area over the area a, draining through a point and;

2) that the hydraulic gradient of the saturated zone can be approximated by the local surface topographic slope, tan β.

Thus, the model does not explicitly account for the influence of soil type or land use on runoff. There are several problems that are often encountered with TOPMODEL. Grid squares that are large in comparison to hillslope lengths cannot be used to derive meaningful values for the topographic index. Sinks in the DEM can also cause problems. Sinks occur where a grid cell(s) elevation is lower than the surrounding cells (Bedient and Huber, 2002). These can be the result of DEM errors or they may represent real depressions or ponds (Beven, 1997).

TOPMODEL has been used in numerous studies and has generally performed well. It has also been praised for its simplicity, being characterized by only 3 parameters and an index curve. It is easy to apply and allows users to visualize the effect of each parameter (Francini et al., 1996). Holko and Lepisto (1997) used TOPMODEL to simulate the hydrological behaviour of a mountain catchment. They reported that the overall simulated runoff volume was close to the measured value. However, peak runoff was generally overestimated, which the authors attribute to their use of a single melt factor and their snow model's confusion of some snowfall with rainfall. Blazkova and Beven (1995) used TOPMODEL to estimate flood frequency curves for three small

catchments in the Czech Republic. They used a stochastic rainfall model to generate input data sets, which were checked against measured data. Their flood frequency curves were constrained using regional estimates and measured series' for short return periods. They also calibrated TOPMODEL by adjusting the average effective transmissivity. Citing the need to understand hydrological processes in humid, tropical environments, Molicova et al. (1997) tested TOPMODEL's applicability in a 1-hectare catchment in French Guiana. They reported differences between recorded runoff and simulated runoff of 0 and 4 mm for rainfall depths of 54 and 57 mm respectively.

Other authors have augmented or improved upon the original TOPMODEL. Beven and Freer (2001) implemented a kinematic wave method for routing subsurface flow to replace the original scenario of a quasi-steady state saturated zone. This allows more flexibility in the definition of hydrologically similar points. Lamb et al. (1997) introduced a generalized saturated zone formulation to be used in place of the original exponential function and tested it on a catchment in Norway for which detailed water table data were measured. They found the method to be just as efficient as the original formulation and it requires one less parameter to be calibrated.

While simple and generally effective, TOPMODEL has some noteworthy limitations. Guntner et al. (1999) found that, while the model generally produced satisfactory estimates of runoff, inadequacies of the model structure in relation to contributing area of saturated overland flow exist. Additionally, there is no easy way to incorporate GIS functionality into the model framework. However, Huang and Jiang

(2002) managed to integrate TOPMODEL functionality into ArcView by rewriting the appropriate equations in Avenue.

2.1.2 GIBSI

The Gestion Intégrée des Bassins versants à l'aide d'un Système Informatisé (GIBSI) is a comprehensive model that evaluates water quality as well as runoff. The basic components are a database that includes spatial and attribute data, and physically-based hydrological, soil erosion, agricultural-chemical transport and water quality models (Rousseau et al., 2000).

No GIBSI applications except for the pilot project have been reported in the literature to date. The initial calibration of the model was performed using data from the Chaudière River which is south of Quebec City, Quebec (Mailhot et al., 1997). Model validation used measured data from the same river basin. Rousseau et al. (2000) published an update on the progress of the model. They reported that water yields simulated by GIBSI were always within 15% of observed values for both the calibration and validation periods.

2.1.3 MMS

The Modular Modelling System (MMS) is designed to be customized by users to suit their specific needs. Users build their own model by selectively coupling the

appropriate process algorithms or designing new ones in the case that no module exists for some process. The model framework has three primary components: pre-process, model and post-process. The pre-process component includes tools for inputting, analyzing and preparing spatial and time-series data for input into the model. This allows the user to simulate variation of model parameters both geographically and temporally. The model component is the core component where the user selectively links process modules. Finally, the post-process component includes tools to display and analyze model results (Markstrom, 2000). Effective user-defined modules should 1) relate directly to real-world components or processes, 2) have input and output variables that are measurable values and 3) communicate solely via these input and output variables (Leavesley et al., 2002).

Wilby et al. (1999) used MMS in a unique study to validate a General Circulation Model (GCM). Using the Animas River, Colorado as a test basin, statistical downscaling techniques were used to derive MMS inputs from the GCM. Runoff volumes were simulated for the period 1987-1994 with errors of 2 to 12%.

2.1.4 PCRaster

PCRaster integrates environmental modelling functions with classical GIS functions in a raster-based, comprehensive model. A geostatistical module is integrated with the GIS component of the model. The model treats watersheds as sets of discrete information cells that can exchange data with their neighbours. GIS or modelling

operations are treated as functions that change the properties of the cells. These changes are based on the relationship between attributes in one cell or between cells. Functions are built and executed using the Dynamic Modelling Language (DML), a special purpose computer language designed specifically for environmental modelling. More than 120 spatial and temporal operators (i.e. Boolean, conditional, filtering, geomorphological and hydrological operators) are included with the model (Van Duersen et al., 1995).

PCRaster has been used in a variety of studies. Van der Perk et al. (1998) built a series of functions using DML to model the spatial and temporal variation of radio-caesium concentrations in alluvial and peaty soils resulting from the Chernobyl explosion. Svetlitchnyi et al. (2003) used PCRaster to model the average seasonal spatial distribution of soil moisture content on slopes and small catchments. They estimated the relative moisture content of the upper 50 cm of soil in summer as a function of the form of relief, longitudinal slope profile shape, aspect, slope gradient and the relative distance from the divide. Model verification using field data resulted in a Root Mean Square (RMSE) error of 0.073 or 7.2% of the average wetness coefficient. De Roo et al. (1999) built a model in PCRaster that simulates river discharge based on topography, soils and land cover. Karssenberg (2002) designed a process-based hydrological model to assess the suitability of programming languages for hydrological modellers. His primary complaint was that the DML, like all environmental modelling languages, is easier to comprehend for a non-computer science specialist but is poorer in generic application and performance than system programming languages. Thus, it is best suited to development of new models that can be tailored to modelling aims and available field data.

2.1.5 SWMM

The United States Environmental Protection Agency's Storm Water Management Model (SWMM) is a rainfall-runoff simulation model that was designed primarily, but not exclusively, for the high runoff from urban environments. Flow routing is performed for surface and subsurface conveyance and groundwater systems. The system can also simulate non-point source runoff quality and routing as well as storage, treatment and other best management practices. New versions of the software have been created for various purposes, including an ArcView link that allows users to visualize the model in conjunction with existing GIS data (Huber and James, 2003).

There have been a few applications of SWMM in the literature. Zaghloul and Abu Kiefa (2001) used neural network software to calibrate the model, thereby avoiding the lengthy process of obtaining appropriate physical and hydrological parameters. Tsihrintzis and Hamid (1998) used SWMM to simulate the quantity and quality of urban storm water runoff from four small catchments in Florida. The purpose of the study was to test the model's applicability in small subtropical urban catchments. Their predicted hydrographs and pollutant loadings showed good agreement with measured values.

2.1.6 WMS

The Watershed Modelling System (WMS) was designed to be a comprehensive hydrologic modelling environment. The software performs watershed and sub-basin

delineation, geometric parameter calculation, hydrologic parameter calculation and result visualization. Users can import soil type and land use data as well as Triangular Irregular Networks (TIN) or DEMs for basin delineation with the Map module. WMS has interfaces to several external hydrologic models and contains tools to calculate Lag Time (time from centre of mass of rainfall excess to the peak of the hydrograph) and Time of Concentration (time for a wave to propagate from the most distant point in a watershed to the outlet) (Environmental Modelling Systems, 2002).

The designers of WMS claim that it is used by hundreds of firms across the globe (Environmental Modelling Systems, 2002). However, there are few published references to the model. The United States Army employed WMS in Bosnia in 1997 to produce stage forecasts for the Sava River. They used meteorological observations, numerical models and 2-hour delay river gauge readings as inputs. Predictions for two cross-sections were within 10 cm of measured data for stages of 8 to 10 m (Sands, 1997).

2.2 Integration of GIS, Remotely Sensed (RS) Data and Flood Forecasting Models

2.2.1 GIS Inputs

Spatial data and GIS have been used in flood forecasting to various degrees. Some simple raster-based models have been successful. Horritt and Bates (2001a) compared a basic raster-based model to a more complex finite-element approach for predicting floodplain inundation and found that they performed equally well. Bates and De Roo (2000) used a similar model based on a high resolution DEM. They were able to

accurately predict 81.9% of inundated and non-inundated areas for a flood that occurred on the Meuse River, Netherlands in 1995. Both studies emphasized that raster models are relatively simple and easy to calibrate. However, simple raster models do not offer the intrinsic visualization tools, nor the ability to easily incorporate other data sets (soil type, land use, population) that a full GIS software package does (Al-Sabhan et al., 2002). Thus, the use of a DEM in a GIS-based model offers more flexibility while incorporating the simplicity of a raster-based terrain modelling approach. The resolution of the data must be considered for such an approach because coarse resolutions can lead to errors, particularly with respect to flood wave travel times (Horritt and Bates, 2001b).

Flood forecasting models that use GIS fall into two general categories: loosely coupled and tightly coupled. In a loosely coupled model, a GIS is linked to an external flood forecasting model where operations are performed in a computer language that is best suited to the task. Tightly coupled models are developed within a GIS environment using a macro-language (Al-Sabhan et al., 2002). Examples of tightly-coupled models include WMS and PCRaster, which have fully integrated GIS components.

One common use of loosely coupled models is to create inputs for a flood forecasting model. Correia et al. (1998) used a GIS to create inputs for two different models and found that the software was quite flexible in this respect. Several other authors have used loosely coupled models including Hromadka II and Yen (1996), Jain et al. (2000), and Lacroix et al. (2002).

There have been other studies that have evaluated the usefulness or validity of using GIS for environmental modelling applications. De Roo (1998), while reviewing runoff erosion models, noted that GIS-based models do not necessarily produce better results than much simpler, spatially lumped models although they reproduce topography in greater detail. The author attributes this partly to the uncertainty involved in estimating and measuring the large number of input variables at a catchment scale. Hwang et al. (1998) stressed that uncertainties in results from GIS, which are not generally provided, should be assessed to facilitate more accurate GIS-based modelling. Karimi and Houston (1996) cited the advantages of custom GIS functions including:

1) reduced time spent subjectively evaluating data;
2) the provision of consistent results between modellers, and;
3) the allowance of rapid and regular variation of input data.

They also suggest that to maximize the usefulness of GIS for environmental modelling, the GIS programming environment should be easy to use and support capabilities similar to those available in programming languages. Sui and Maggio (1999) argued that conceptions in space and time that are embedded in current versions of GIS are not compatible with those in hydrological models. They call for the development of a new, high level common ontology that would incorporate alternative conceptualizations of space and time capable of handling cross-scale linkages of hydrological processes. They conclude that such a data framework, which would be compatible with GIS and hydrological models, would remove some of the current constraints on the types of models that can be developed.

Other authors have developed unique methods for integrating GIS and hydrological models. McKinney and Cai (2002) used an object-oriented approach to integrate a GIS with a water resources management model. Greater flexibility was created by integrating data, models, and user interfaces in the GIS environment. Coroza et al. (1997) used a GIS interface to increase the accessibility of an engineering runoff model to planners without substantial hydrologic expertise. The visual display was much improved and results obtained with the linked system were not significantly different than those obtained from the conventional model. Carpenter et al. (1999) used a GIS to help create an improved flash flood warning system. This was done by using models of channel geometry developed in the GIS to estimate threshold runoff (the amount of excess rainfall that is sufficient to cause flooding at the basin outlet) for basins across the United States. They obtained threshold runoff values ranging from 9.5 mm to 34 mm for hourly rainfall durations. When these values were compared with manually computed unit hydrographs, a maximum difference of 15 mm was obtained. The authors attribute the bulk of the errors to uncertainty in the calculation of unit hydrographs and estimation of channel cross-sectional properties. Thus, they were confident in the accuracy of their GIS-based procedure. Daviau et al. (2000) used kriging and other geostatistical techniques to map regions with homogenous flood frequency. They used a number of different data sets as indicators of flood frequency including climate, vegetation, topography and flood timing and magnitude statistics. The results were integrated in a GIS and validation tests were performed. The authors concluded that maps of mean and variance for flood frequency and magnitude could serve as indicators of climatic influences on flood generating mechanisms.

2.2.2 Remotely Sensed Imagery Inputs

Remotely sensed images have also been used to create inputs for flood forecasting models. Portman (1997) used remotely sensed images of the 1993-1994 floods on the Rhine River in conjunction with a GIS to develop a warning system. The author reported results that were initially promising but cited the need for ground truth data for further validation. Bates et al. (1997) used a similar technique to demonstrate the potential of remote sensing to aid in parameterization and validation of flood forecasting models.

Another application of remote sensing is to estimate vegetation or land cover, which has an impact on the rainfall-runoff response of land units. Yin and Williams (1997) developed an empirical model to convert values of the Normalized Difference Vegetation Index (NDVI) as estimated from classified satellite images to Leaf Area Index (LAI) values. The LAI is broadly defined as the amount of leaf area in a vegetation canopy per unit land area (Scurlock et al., 2001). Melesse and Shih (2002) used Landsat images to create land use maps. These were in turn used to determine curve numbers. In this way, classified satellite images could potentially be used to create a full set of inputs for a flood-forecasting model, which might otherwise be derived from several sources (i.e. soil, land use, and vegetation data). With high-resolution images (i.e. from Systeme pour l'Observation de la Terre) one could also obtain a very high-resolution watershed model.

2.3 Use of the Curve Number Method

The Curve Number Method is an empirical method for converting rainfall into runoff. Curve numbers range from 30 to 100 and represent the amount of rainfall required to exceed the surface storage capacity of a given land unit. They are defined based on soil type, land use, and ground cover. The Curve Number Method has been used in several studies. Melesse and Shih (2002) used Landsat images to map curve numbers in South Florida. Although they did not verify the results, they outlined a method for using satellite imagery to map curve number distributions. Mack (1995) introduced a computerized version of the Curve Number Method. The model features standardized calculation methodology, generates reproducible results and allows for the rapid calculation of runoff estimates. Osterkamp and Friedman (2002) used the Curve Number Method in their study of the disparity between extreme rainfall events and rare floods in the semi-arid American west and in more humid environments. They found that high curve numbers in semi-arid areas are the result of soil and vegetation that limit infiltration and enhance runoff.

2.4 Effects of Tillage on Rainfall and Snowmelt Runoff

Tillage can impact the duration and intensity of flood hydrographs in a watershed by diverting or attenuating overland flow (Eaglin, 1996). Thus, surface runoff may not flow down the steepest slope gradient where tillage is present, which could invalidate an assumption made in most flood forecasting models. Tillage effects have been fairly well

documented in the literature. Hansen et al. (2000) studied the effects of three different tillage systems (fall moldboard, chisel ploughing with spring disking, and ridge tilling) on runoff. They found that the percentage of available water that ran off ranged from 50 to 80%. Takken et al. (2001) built two erosion models for a watershed based on topography and tillage respectively. They reported that the latter pattern simulated erosion patterns more closely. They also noted that higher erosion rates were simulated using the topography model because the average slope was higher and contributing areas where larger. Souchere et al. (1998) reported that runoff flows over more than 50% of 20 out of 23 agricultural catchments were along tillage directions. In a similar study of agricultural catchments, Takken et al. (2001) found that flow was in the direction of tillage for over 75% of the areas they observed. Also noteworthy is research by Martin (1999) who investigated the potential of using tillage to reduce flood risk. The author reported that some, but not all intercrop management methods reduced runoff and thus have flood mitigation potential.

Not all tillage patterns have the same effect on runoff, although some do (i.e. Hansen et al., 2000). Since tillage patterns can change from year to year, it must also be assumed that the effect of tillage on overland flow is temporally variable. The variability of tillage's impact on runoff may mean that this phenomenon is hard to quantify or account for with respect to modelling runoff.

Chapter 3: Methodology

3.1 Watershed Model Development

3.1.1 HEC-GeoHMS Watershed Pre-Processing

The Watershed Pre-Processing tools in HEC-GeoHMS where used to delineate streams and sub-basins for the Duffins Creek Watershed using a 30-metre resolution DEM (original data source: Canadian National Topographic Database) from DMTI Spatial (DMTI Spatial, 2002). Watershed Pre-Processing consists of a total of nine steps. First, HEC-GeoHMS fills sinks on a cell-by-cell basis to enable runoff direction simulation. If any cell has a lower elevation than the eight surrounding cells, its elevation is increased to that of the lowest neighbour. Flow Direction is then calculated for each cell using an eight-point pour algorithm. Eight possible flow directions are considered by the algorithm (north clockwise through to northwest) and the steepest downslope gradient is taken as the flow direction. The results of this algorithm are used to calculate flow accumulation, in which the number of upstream cells draining to each respective cell is summed. Upstream drainage area can be easily calculated from this value by simply multiplying the number of upstream cells by the area of one cell. The next step is Stream Definition, which requires the user to specify a threshold for stream initiation. This value is the minimum contributing area (in cells or squared distance units) required for stream initiation. The default value, which is 1% of the total drainage area, produced good results in comparison with a map of the Duffins Creek stream channels (Figure 3.1). Experimentation with other values could potentially have produced a better result, but given the scope of this project and the potential improvement upon error, this was not

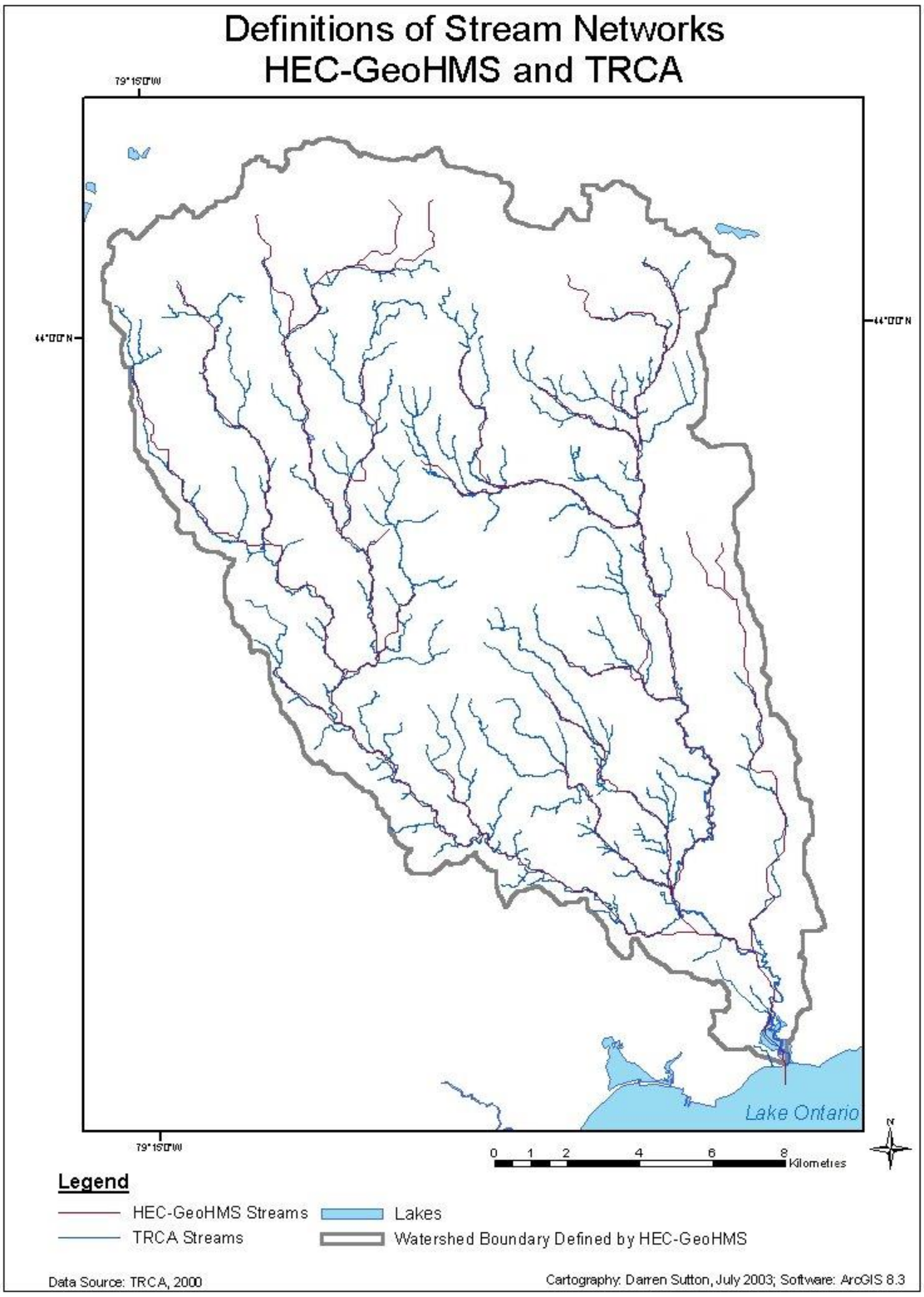

Figure 3.1: Comparison of Duffins Creek Stream Networks Defined by HEC-GeoHMS and the TRCA

viewed as an effective use of time. Stream Segmentation divides the stream into a series of links. These are defined as sections of the stream that connect two successive junctions, a junction and an outlet, or a junction and the drainage divide. Watershed Delineation defines a sub-basin for each stream link. The result is a grid of sub-basins that cover the watershed. Watershed Polygon Processing converts this grid file into a Shapefile where all sub-basins are represented as polygons. Stream Segment Processing performs a similar operation to convert all stream segments into lines that are stored in a Shapefile. The final step, Watershed Aggregation, aggregates sub-basins at every stream confluence to improve computation performance and enhance data extraction (Doan, 2000). For the Duffins Creek Watershed, the result was a set of 45 sub-basins (Figure 3.2).

Automated watershed delineation using a method such as HEC-GeoHMS Watershed Pre-Processing is only one option available for defining watersheds and stream networks. Both procedures could also be accomplished manually using stereographic pairs of aerial photographs (Garcia and Camarasa, 1999), although this would be much more time consuming. Some limitations of automated watershed delineation methods have been identified. Garcia and Camarasa (1999) tested an automatic extraction technique that used PCI Inc. Software Version 6. They found that the method performed well for catchment headwaters, but was not as effective for middle and lower reaches. The rate of coincidence between a manually delineated watershed and the PCI procedure was 62.2% for headwaters but ranged from 14.5 to 1.5% in the lower reaches. Martz and Garbrecht (1998) cited closed depressions and flat areas as being two

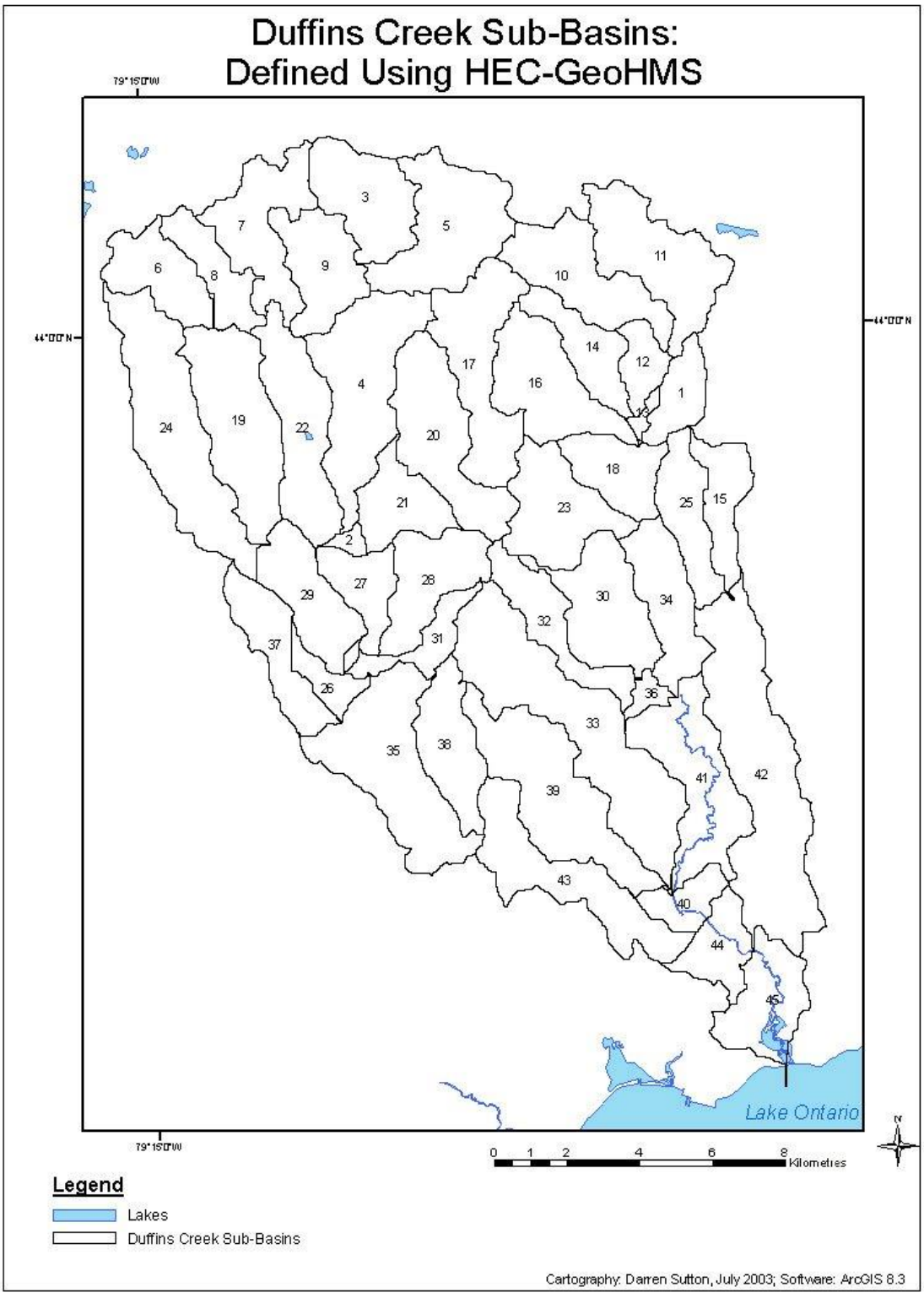

Figure 3.2: Sub-basins in the Duffins Creek Watershed as Defined by HEC-GeoHMS Watershed Pre-Processing

problem areas for watershed delineation using DEMs. Closed depressions are generally the result of DEM errors while the eight point pour algorithm often encounters problems when calculating flow directions across flat areas. Therefore, while automated watershed delineation is quicker and easier than manual delineation, some problems exist that may lead to errors.

3.1.2 Land Cover and Soil Type

Hydrological response units were defined as collections of grid cells with the same curve number. To facilitate overlay with soil and land cover data sets, a Digital Elevation Model (DEM) of the watershed was converted to a point Shapefile using an Avenue Script called Grid2Point (Ardron, 2000). Shapefiles of land cover and soil type (including hydrologic soil group) were obtained (TRCA, 2000). Land cover data included estimations of the percentage of each urban unit that is impervious, which were useful in determining curve numbers for urban land. The spatial boundaries of these Shapefiles correspond to the Duffins Creek Watershed boundary as defined by the TRCA. This boundary is slightly smaller than the boundary defined using HEC-GeoHMS (283 km^2 compared to 298 km^2). It is difficult to say whether the difference is the result of overestimation by HEC-GeoHMS or underestimation by the TRCA or both. However, there are few large continuous areas that were included by HEC-GeoHMS and omitted by the TRCA (Figure 3.3). The 16 km^2 over which the two definitions disagree represents a percent difference of only 5.3%, indicating that both boundaries are for the most part in agreement.

Figure 3.3: Difference Between Duffins Creek Watershed Boundaries Defined by the TRCA and HEC-GeoHMS

Due to the small difference in boundaries, soil and land cover data supplied by the TRCA were augmented using the Durham County Soil Survey (Webber *et al*., 1946) and the Ontario Land Cover Database (Ontario Ministry of Natural Resources, 1998) respectively. The Ontario Ministry of Natural Resources (OMNR) data are two years older than TRCA's land cover data, which may have led to some errors. There has likely been little change in the distribution of soil type since the Durham County Soil Survey was published. A wide variety of land cover classes were used in the OMNR data. These classes were easy to synchronize with the relatively few classes used by the TRCA. In the case of soil type, synchronization was performed largely by spatial association of polygons. This is because soils were defined primarily in terms of grain size and horizon sequences so some interpretive knowledge of soils would be required to deduce their infiltration properties. Aggregated land cover and hydrologic soil group maps were produced by expanding the TRCA Shapefiles based on the Durham County Soil Survey and OMNR data (Figures 3.4 and 3.5).

3.1.3 Ground Cover and Tillage Practices

To assign curve numbers to forest, wetland and urban open space, an estimation of the percent of ground that is covered by vegetation is required. To assist in defining these curve numbers, the Leaf Area Index (LAI) was calculated for the Duffins Creek Watershed. Yin and Williams (1997) outline a procedure, which uses a map of Normalized Difference Vegetation Index (NDVI) to estimate the LAI index. The NDVI

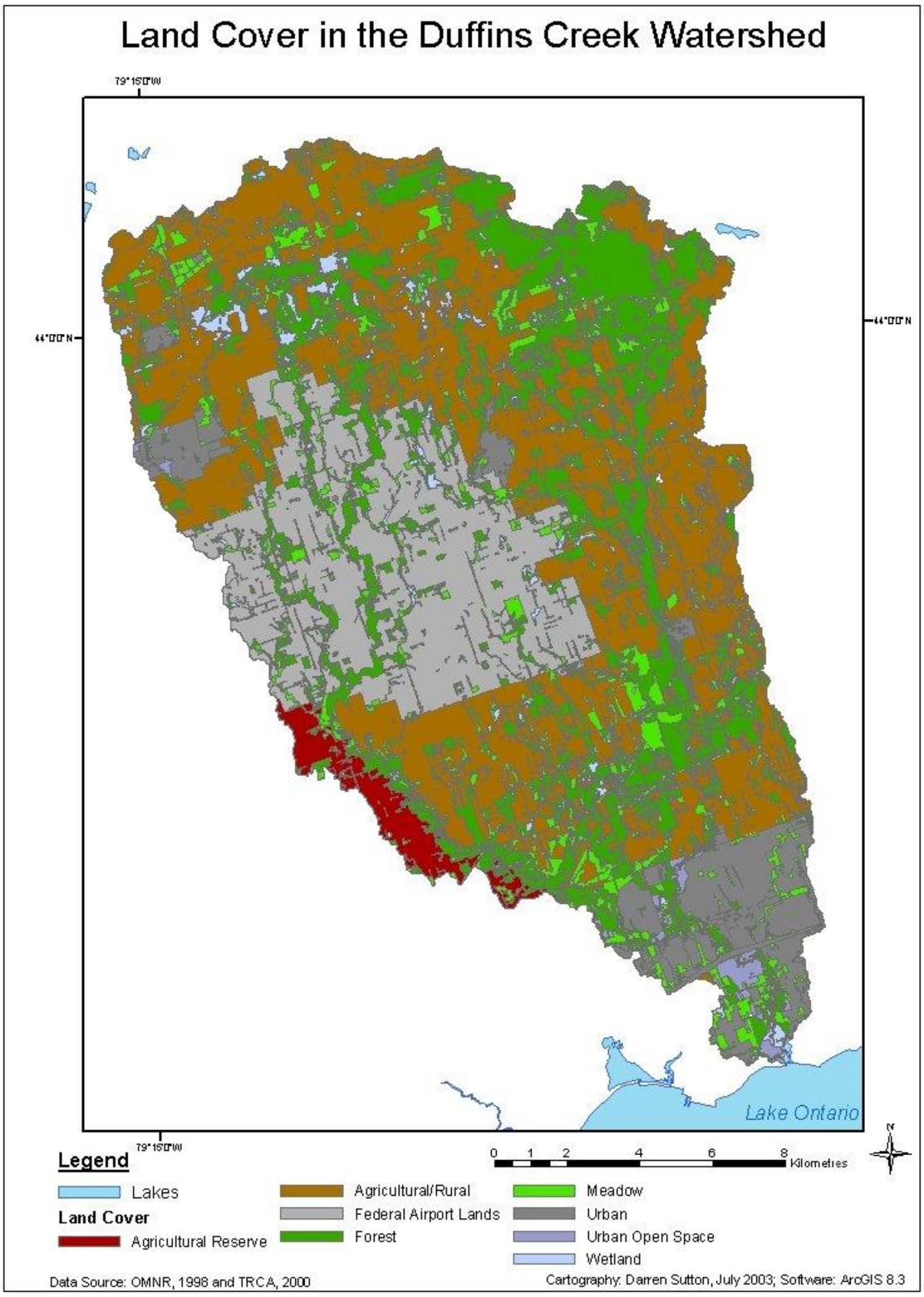

Figure 3.4: Land Cover in the Duffins Creek Watershed, Assembled from TRCA and OMNR Data

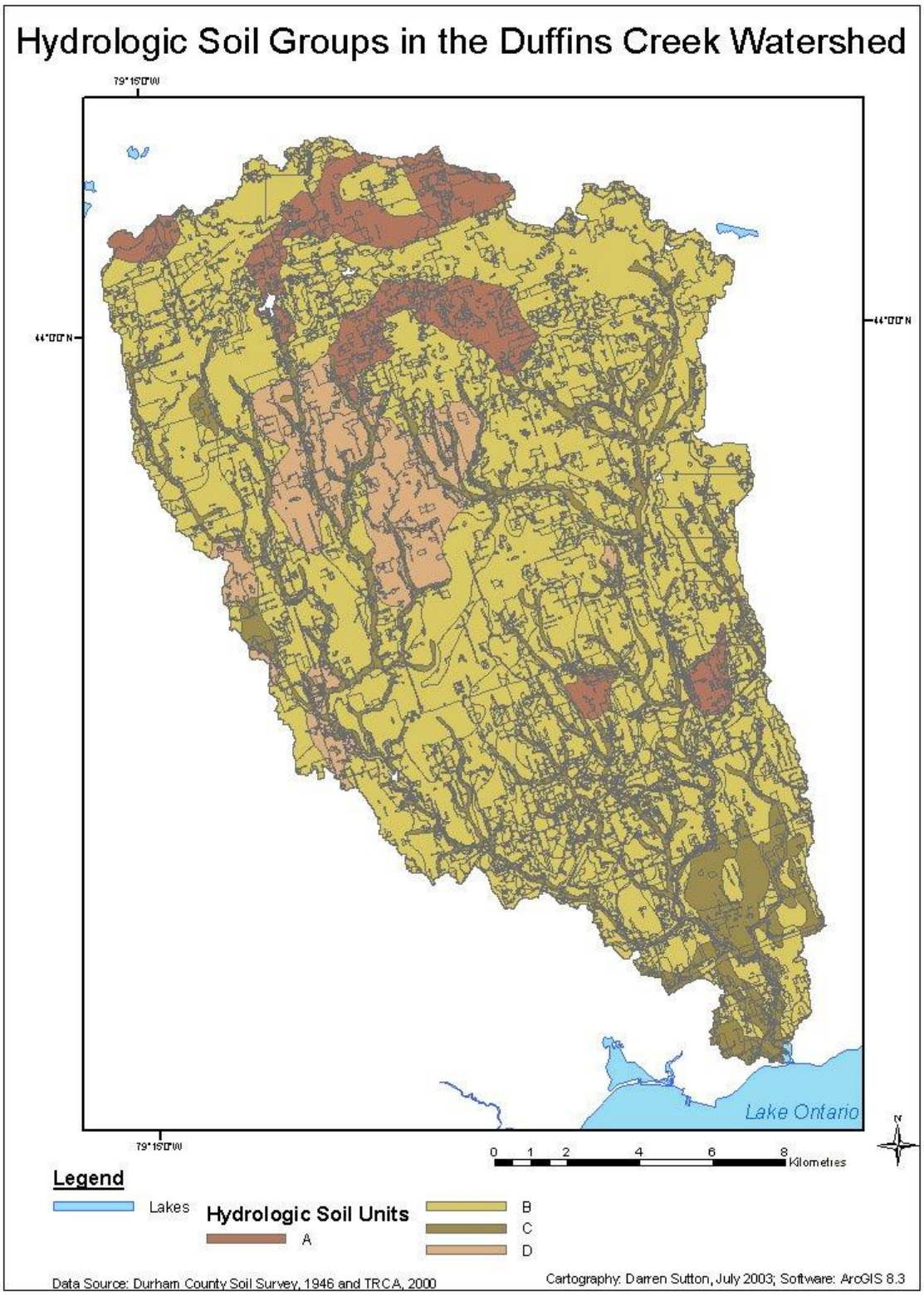

Figure 3.5: Hydrologic Soil Groups in the Duffins Creek Watershed, Assembled from the Durham County Soil Survey and TRCA data

for Landsat Enhanced Thematic Mapper + (ETM+) data is calculated using:

$$NDVI = (Band4 - Band3)/(Band4 + Band3) \quad (29)$$

(Lillesand and Kiefer, 2000). NDVI for this research was computed from a Landsat 7 ETM+ image from June 10, 2000. LAI is derived from NDVI using:

$$LAI = LAI_{max}(NDVI-NDVI_{min})/(NDVI_{max}-NDVI_{min}) \quad (30)$$

A value for LAI_{max} was determined based on Arnold *et al*. (1990). The authors produced a map of average LAI_{max} values for the conterminous United States. All northern states East of Minnesota have an average LAI_{max} of 5. Since it seems to be nearly ubiquitous in the Eastern USA, a value of 5 was assumed to be representative of Southeastern Ontario as well. This assumption is also based on the fact that the northern states bordering Ontario are relatively close to the study area.

$NDVI_{max}$ and $NDVI_{min}$ where obtained from the results of the NDVI calculation and were used to compute LAI for the study area (Figure 3.6). Land cover data (Figure 3.4) was combined with LAI data to determine ground cover for forest, wetland, and urban open space.

The curve number of agricultural land depends on whether conservation tillage (contoured or terraced) is in practice. To determine the tillage practices at work in the

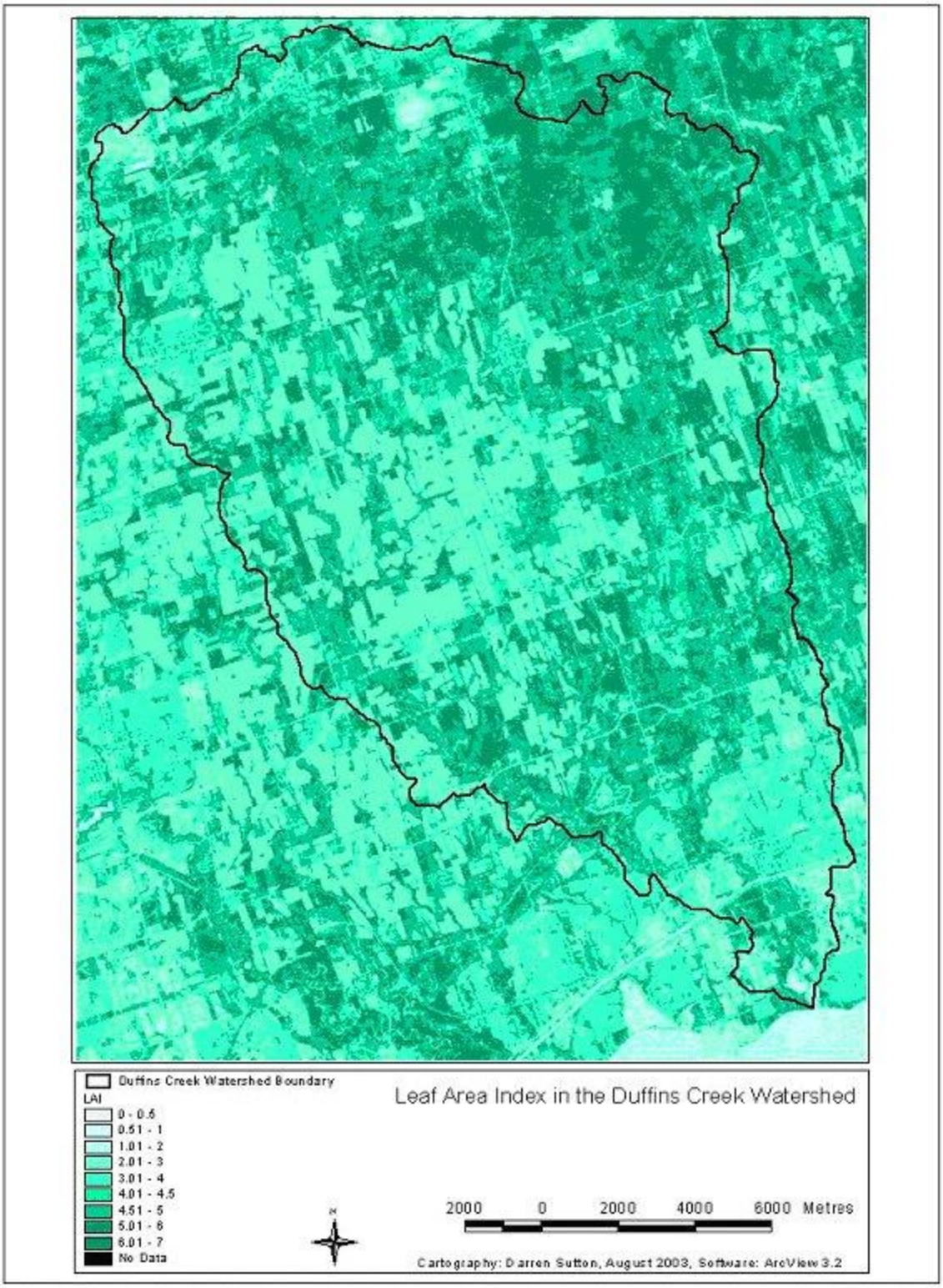

Figure 3.6: Leaf Area Index (LAI) in the Duffins Creek Watershed

Duffins Creek Watershed, digital orthophotographs covering the majority of the study area were obtained (Triathlon Mapping Corporation, 1995). Examination of these orthophotographs revealed tillage lines along contours of hilly crop land (Figure 3.7). Much of the watershed has a low slope gradient and so conservation practices are not necessary on many fields. It was assumed that runoff on agricultural land was influenced by contour tillage because most slopes appear to be tilled. Curve numbers were assigned accordingly.

3.1.4 Curve Number Distribution

A complete map of curve numbers in the Duffins Creek Watershed was created by combining data on land cover, soil type, LAI and tillage practices (Figure 3.8). Curve number 71 covers the largest area by far while curve number 55 also accounts for a significant portion of the study area (Table 3.1).

Subsequent analysis of the TRCA's soil type and land cover shapefiles revealed that they are projected as North American Datum (NAD) 1927 whereas other data used for this project are in NAD 1983. As a result, hydrological response units are misplaced by approximately 15 metres to the West (based on visual comparison of original shapefiles with reprojected versions). This could have a slight impact on travel time predictions.

Figure 3.7: Example of Contour Tillage in the Duffins Creek Watershed (note arrows which identify tillage lines along the edge of the field)

3.2 Calculation of Travel Time

3.2.1 Overland Flow

Travel times for overland flow were calculated for each sub-basin. It was assumed that runoff from all points enters the river channel at the outlet of each respective sub-basin. An assumed error in the HEC-GeoHMS algorithm resulted in one basin (Basin 8 – see Figure 3.2 for basin numbers) not containing a stream channel outlet. As such, this

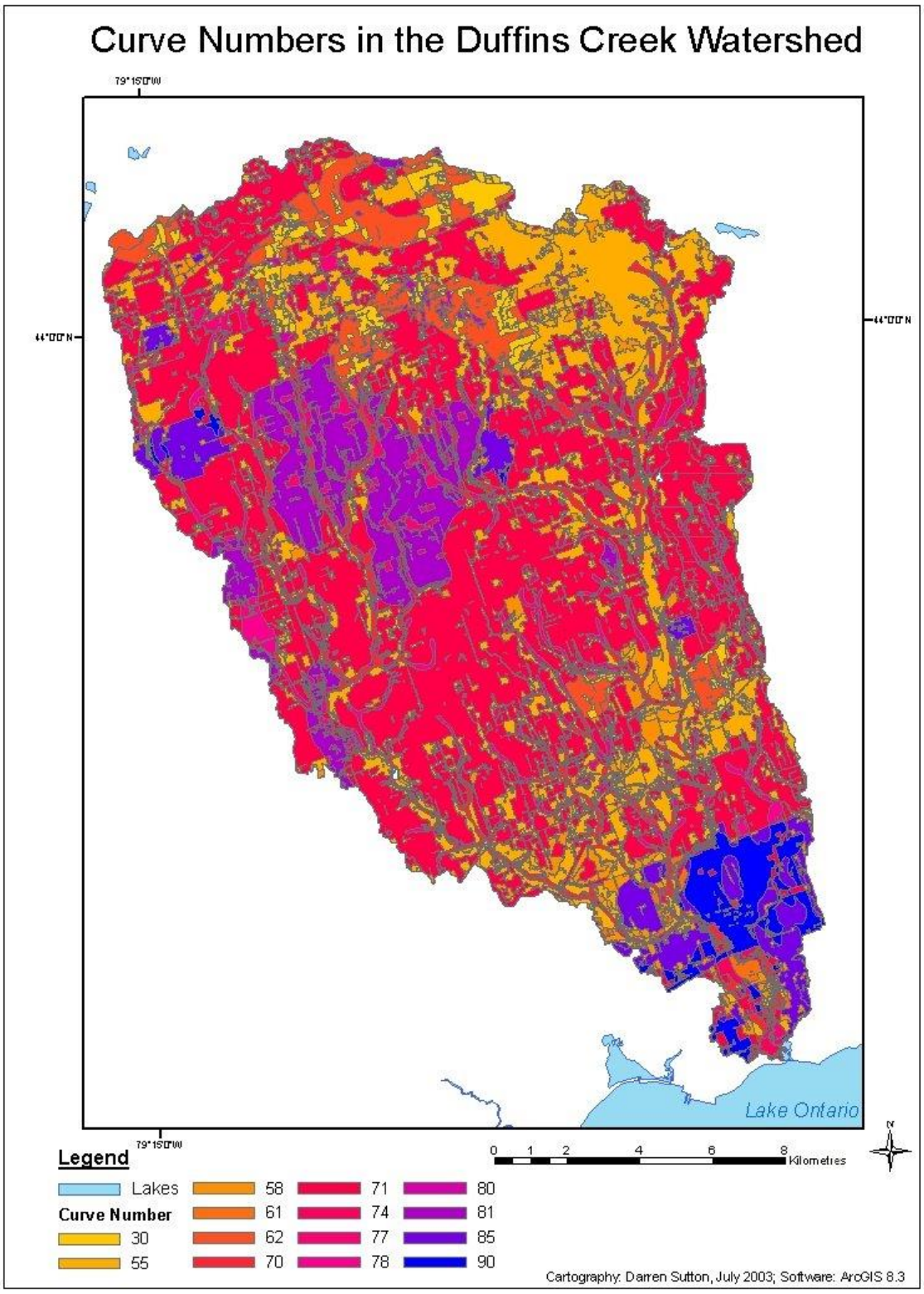

Figure 3.8: Curve Numbers in the Duffins Creek Watershed

Table 3.1: Curve Numbers in the Duffins Creek Watershed

Curve Number	Total Area (km^2)	Percent of Total Watershed Area
30	8.9	2.9
55	54.8	18.1
58	16.3	5.4
61	1.4	0.5
62	14.3	4.7
70	12.7	4.2
71	131.5	43.5
74	1.2	0.4
77	8.2	2.7
78	12.5	4.1
80	0.9	0.3
81	19.6	6.5
85	11.9	3.9
90	8.1	2.7

basin was merged with the next downstream basin (Basin 19). It was assumed that all runoff from Basin 8 flows overland to the outlet of Basin 19, which may inflate travel times for points in Basin 8.

The most accurate way to calculate travel time for overland flow is to calculate the flow path distance for each point using some variation of the eight-point pour algorithm that would calculate contributing areas by curve number. Such a method proved to be out of the scope of this project in terms of de-bugging because of the number of Visual Basic sub-procedures required. A simpler method using the direct distance to the outlet for each point can be augmented to account for the average affect of each sub-basin's unique topography. This was done by selecting several points in each sub-basin, with an approximately even spatial distribution and calculating the flow path distance using the HEC-GeoHMS Flowpath Tracing Tool. The Flowpath Tracing Tool

creates a line feature representing the flow path calculated using the eight-point pour algorithm. Ratios of direct distance to eight-point pour distance were calculated for each sample point. The variances of the ratios for each sub-basin are used as indicators of the accuracy of this method (Table 3.2). Low variances were obtained in most cases, suggesting that flow distances can be approximated by multiplying direct distance by the eight-point pour/direct distance ratio.

In general, sheet flow persists for 92 meters after the inception of runoff (Eaglin, 1996), after which it travels as shallow overland flow to the sub-basin outlet. Values of Manning's Roughness Coefficient for sheetflow were determined based on land cover at the point of origin (Table 3.3). Values were obtained from Eaglin (1996).

3.2.2 Channel Flow

Channel Flow travel time was computed on a point-by-point basis. The average hydraulic radius was calculated using flood discharge data for the main branch of Duffins Creek obtained from the TRCA (2002) (Table 3.4). A Velocity-Discharge Curve was defined using these data (Figure 3.9). A third order polynomial trend resulted in a good fit. Baseflow velocity was determined using the velocity-discharge trendline (Figure 3.9) and a baseflow discharge value estimated from TRCA (2002). This resulted in estimations for baseflow discharge of 3.5 m^3/s and baseflow channel velocity of 1 m/s.

Table 3.2: Mean Eight Point Pour Distance/Direct Distance Ratios for Duffins Creek Watershed

Sub-Basin	Mean Ratio	Variance
1	1.30	**0.01**
2	1.28	**0.01**
3	1.97	**0.19**
4	1.30	**0.00**
5	1.40	**0.02**
6	1.19	**0.00**
7	1.41	**0.04**
9	1.48	**0.06**
10	1.48	**0.05**
11	1.29	**0.01**
12	1.26	**0.01**
13	1.31	**0.01**
14	1.23	**0.00**
15	1.25	**0.01**
16	1.25	**0.09**
17	1.34	**0.02**
18	1.29	**0.02**
19	1.27	**0.02**
20	1.41	**0.03**
21	1.34	**0.11**
22	1.23	**0.01**
23	1.31	**0.01**
24	1.35	**0.04**
25	1.23	**0.01**
26	1.28	**0.04**
27	1.27	**0.00**
28	1.28	**0.01**
29	1.35	**0.02**
30	1.25	**0.01**
31	1.32	**0.01**
32	1.32	**0.01**
33	1.27	**0.01**
34	1.31	**0.07**
35	1.55	**0.06**
36	1.49	**0.11**
37	1.16	**0.12**
38	1.27	**0.01**
39	1.32	**0.01**
40	1.48	**0.10**
41	1.87	**0.02**
42	1.37	**0.05**
43	1.29	**0.01**
44	1.60	**0.19**
45	1.33	**0.07**
Average	1.35	**0.04**

Table 3.3: Manning's Roughness Coefficients for Calculation of Sheet Flow Travel Time

Land Cover	Manning's Roughness Coefficient (n)
Urban	0.011
Meadow/Urban Open Space	0.15
Agricultural	0.17
Forest	0.4

The hydraulic radius (R) of a channel can be estimated if values for velocity and discharge are known:

$$R = (Q/(0.5\pi v))^{0.5} \quad (31)$$

where Q is discharge and v is channel velocity. This relationship is obtained by simply rearranging the formula for Q where the channel is treated as a half-pipe shape with radius R:

$$Q = 0.5\pi R^2 v \quad (32)$$

Visual inspection of the orthophotographs (Triathlon Mapping Corporation, 1995) indicates that channel size in the East and West branches of the Duffins Creek is (logically) smaller than in the main branch. It is estimated that size decreased by one half. Further, the upper tributaries are smaller than East and West Duffins by approximately the same ratio. Thus, hydraulic radii are assumed to be half as large in the East and West Duffins Creek as in the Main Branch and one quarter as large in the upper reaches. This is based on the assumption that the channels are approximately the shape of half pipes in which case channel width would vary closely with hydraulic radius.

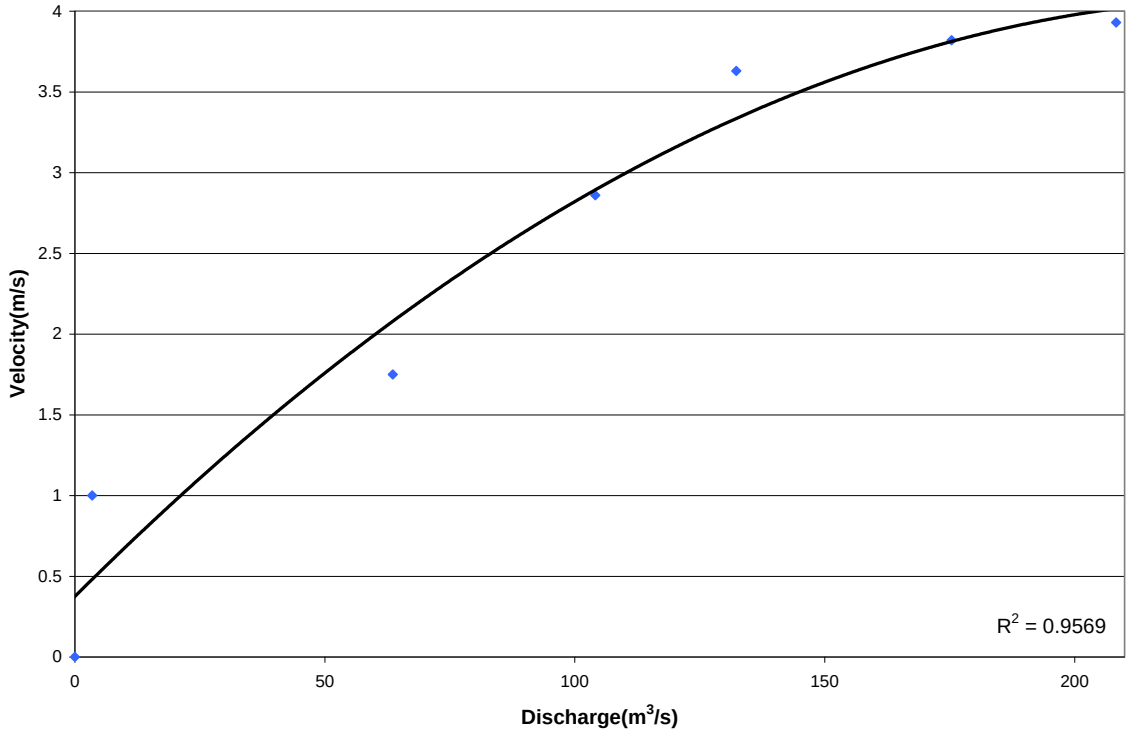

Figure 3.9: Velocity-Discharge Curve for Duffins Creek, Main Branch

Hydraulic radii were estimated using baseflow data and data for floods with recurrence intervals of 2, 5, 10, 25, 50, and 100 years (Table 3.4). The purpose of this was to create a curve similar to a Rating Curve, which is a plot of stage vs. discharge at a channel cross-section (Bedient and Huber, 2002). In this case, hydraulic radius was used in place of stage since no continuous, verifiable records of stage for Duffins Creek were available (Figure 3.10). Third order polynomial trend lines were then fit.

Table 3.4: Peak Discharge and Channel Velocity for Floods on the Duffins Creek, Main Branch (Source: TRCA, 2002a)

Flood Recurrence Interval (Years)	Peak Discharge (m^3/s)	Velocity of Channel Flow (m/s)
2	63.6	1.75
5	104.1	2.86
10	132.3	3.63
25	175.4	3.82
50	208.3	3.93
100	243.6	2.86

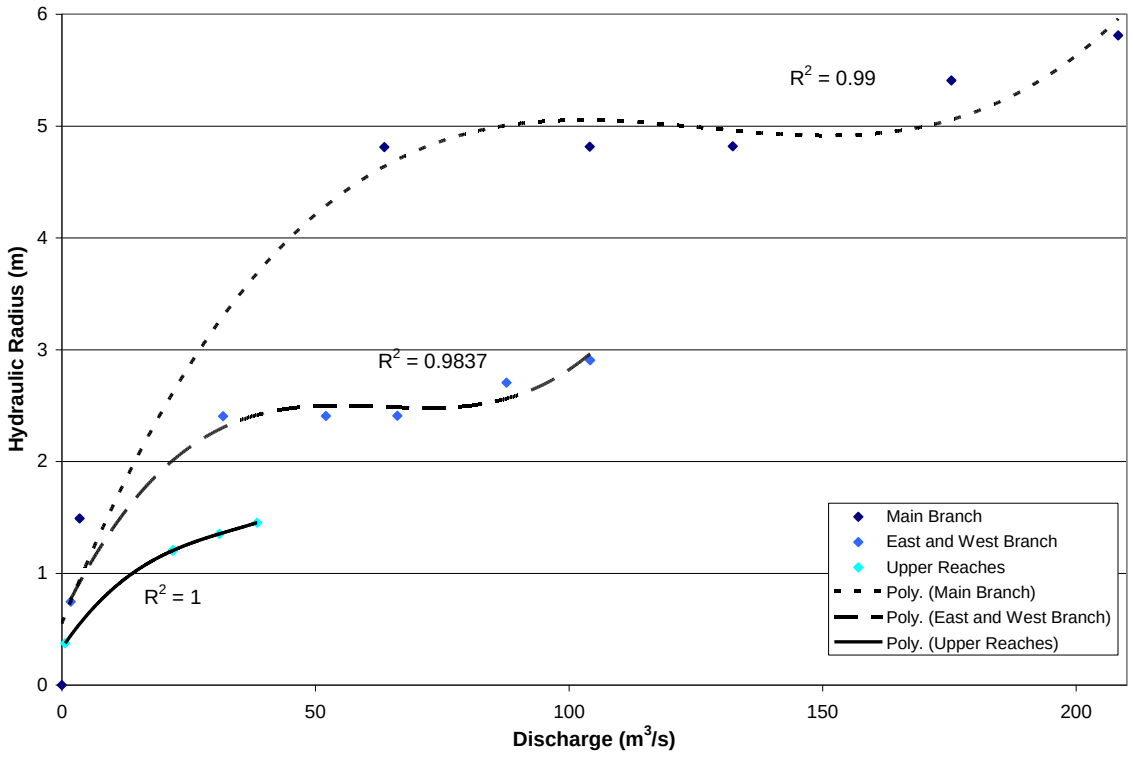

Figure 3.10: Hydraulic Radius-Discharge Curves for Duffins Creek

The form of the trendlines in Figure 3.10 follows the pattern that one would expect. As a channel approaches bankfull discharge, there is no more room for stage to increase until the flow spills over the riverbanks. In this event, hydraulic radius should increase rapidly as flow expands onto the floodplain. These relationships appear to hold

for the Main branch and East and West branch curves in Figure 3.10. It is possible to estimate bankfull discharge using the value at the second inflection point of both curves, although one must accept that this not exact since the trendline is itself an estimate. The curve for the upper reaches does not have a second inflection point indicating that more data points may have been required to produce a full curve.

Figure 3.10 can be used to delineate areas that are in danger of flooding if a DEM is assumed to be representative of watershed topography. In reality, it is known that the DEM consists of a series of flat blocks with widths equivalent to the grid resolution (30 m). If one accepts the limits of the DEM stemming from its resolution then discharge values can be used to estimate the extent of inundation. Effectively, the discharge is divided by the velocity of flow and the number of cells in a channel cross section this volume would fill is assumed to be indicative of the extent of flooding. Maps of inundated areas can be produced for the area around a given cross-section but one must recognize that the stage is derived from a single cross-section. Therefore, inundation upstream and downstream from the cross-section in question could be in error, especially if channel geometry changes significantly.

Six points were selected for model calibration and verification (Figure 3.11). The rationale was to obtain sites that are representative of the East and West Duffins Creek, the main branch of Duffins Creek and the upper tributaries. These points coincide with the outlets of sub-basins where corresponding predictions exist from Visual OTTHYMO. Ideally, the most accurate model verification would be done using gauge data as a control

sample. In this case, a long-term gauge record for the study area was not available. Therefore, the limitations or errors in Visual OTTHYMO had to be accepted.

3.3 Parameters for GAWSER Model

Snowfall, rainfall and mean daily temperature where simulated for use with the GAWSER equations. The use of simulations allows flood forecasts to be produced for different snowpack scenarios where values still agree with one's expectations based on the record of climate normal data. Thus, forecasting is not limited to values from weather gauge records. The Weather Network publishes climate normal data based on 30 years of observations (1961-1991), which can be used to create a simple prediction algorithm. Climate normal data for Ajax are recorded at Toronto's Pearson International Airport, which is the closest available weather station (Tables 3.5 and 3.6).

Table 3.5: Mean Daily Temperature for Ajax, Ontario, Collected at Pearson International Airport (Source: The Weather Network, 2003)

Month	Maximum Temperature	Minimum Temperature	Mean Temperature
January	-2	-10	-6
February	-1	-10	-5
March	4	-4	0
April	12	1	6
May	18	6	12
June	24	11	17
July	27	14	21
August	26	13	20
September	21	9	15
October	14	4	9
November	7	0	3
December	0	-6	-3

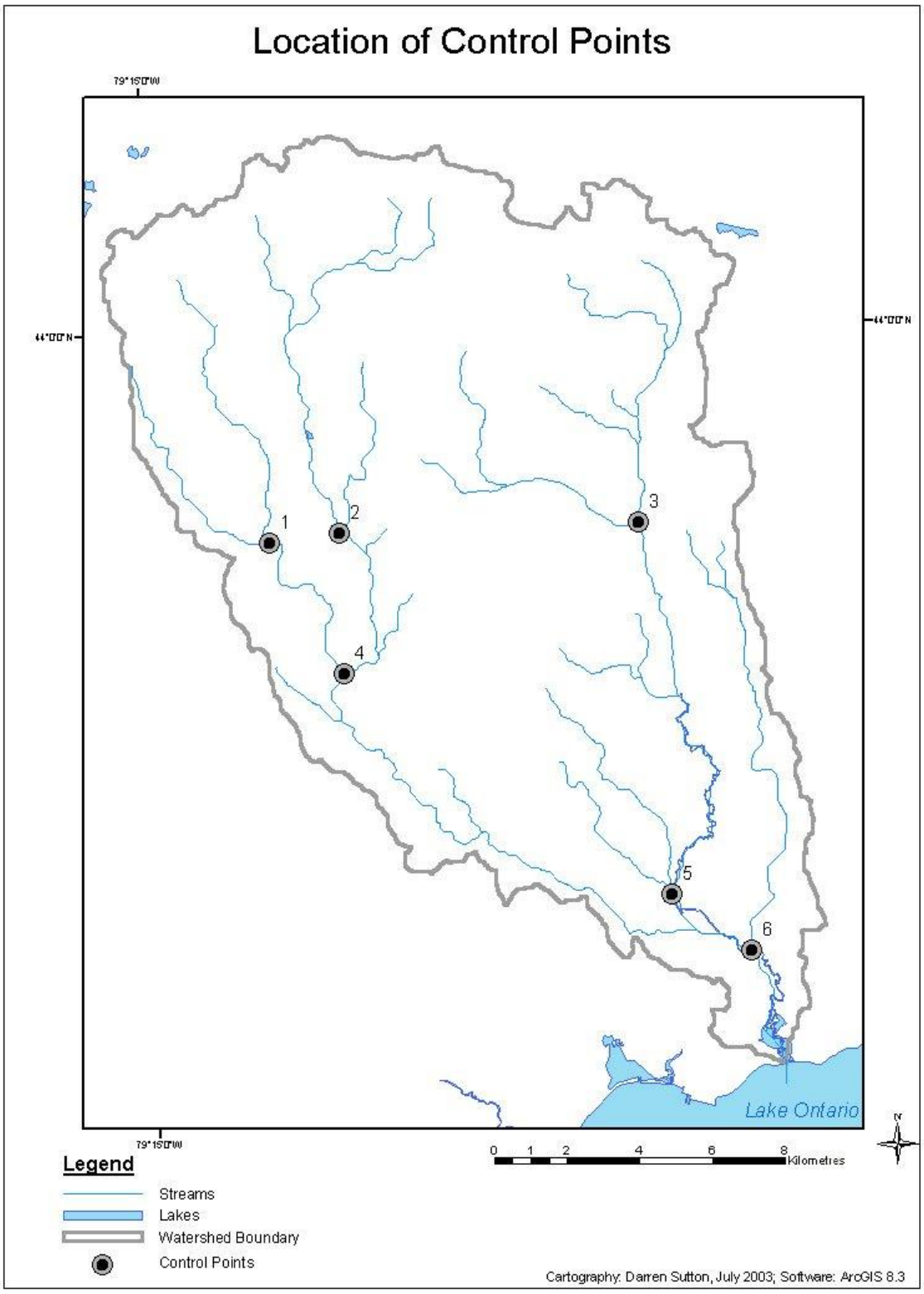

Figure 3.11: Location of Control Points in the Duffins Creek Watershed

3.3.1 Simulating Mean Daily Temperature

Simulation of mean daily temperature for this project is based on the assumption that mean daily temperatures throughout the year are normally distributed. In this case, the number of days in a month when temperature is less than or equal to 0ºC can be divided by the total number of days in the month to obtain a probability. This probability will have a corresponding z-value (Burt and Barber, 1996), which can be used to obtain the standard deviation for each month. This is done by rearranging the standard score formula:

$$z = (x - \mu)/\sigma \tag{33}$$

where x is any temperature value, μ is the mean temperature and σ is the standard deviation. Rearranging this equation to solve for σ where x = 0ºC yields:

$$\sigma = \mu / z \tag{34}$$

where μ is obtained from Table 3.5. The normal curve can be treated as a boundary between temperatures that can and cannot occur in a given month. Temperatures can be simulated using values for z and for the probability density function of a standard normal curve (Burt and Barber, 1996):

$$f(z) = 1/(2\pi)^{0.5}e^{-0.5z\wedge 2} \tag{35}$$

Table 3.6: Climate Normal Data for Ajax, Ontario, Collected at Pearson International Airport (Source: The Weather Network, 2003)

Number of Days Where	Jan	Feb	Mar	Apr	May	Jun
Temp <= 0 °C	30	27	26	15	2	0
Rain >= 02. mm	4	4	8	10	11	11
Rain >= 5 mm	1	1	2	4	4	5
Rain >= 10 mm	0	0	1	2	2	2
Rain >= 25 mm	0	0	0	0	0	0
Snow >= 0.2 cm	12	10	7	3	0	0
Snow >= 5 cm	2	2	1	0	0	0
Snow >= 10 cm	0	0	0	0	0	0
Snow >= 25 cm	0	0	0	0	0	0
Snow Cover >= 1 cm	22	21	11	1	0	0
Snow Cover >= 5 cm	17	16	7	0	0	0
Snow Cover >= 10 cm	10	9	4	0	0	0
Snow Cover >= 20 cm	3	2	0	0	0	0
Number of Days Where	Jul	Aug	Sep	Oct	Nov	Dec
Temp <= 0 °C	0	0	0	7	18	28
Rain >= 02. mm	10	11	10	11	11	7
Rain >= 5 mm	4	4	4	4	4	3
Rain >= 10 mm	2	3	2	2	2	1
Rain >= 25 mm	0	0	0	0	0	0
Snow >= 0.2 cm	0	0	0	0	4	11
Snow >= 5 cm	0	0	0	0	0	2
Snow >= 10 cm	0	0	0	0	0	0
Snow >= 25 cm	0	0	0	0	0	0
Snow Cover >= 1 cm	0	0	0	0	2	17
Snow Cover >= 5 cm	0	0	0	0	0	10
Snow Cover >= 10 cm	0	0	0	0	0	4
Snow Cover >= 20 cm	0	0	0	0	0	1

where e is the base of natural logarithms. The simulations for this project were driven by random integers obtained from a web-based source (www.random.org) that uses atmospheric noise to seed a random number algorithm (Haahr, 1998). Two sets of random numbers were obtained, one of which was constrained to fall between 0 and 0.25066, where the latter is the value of f(z) at the mean of a normal distribution, and the other distributed between -3 and 3 (z-values). An algorithm, which can be seeded, was devised to cycle through both sets of random numbers and extract pairs sequentially. Any

pair of numbers that fall below the normal curve when they are plotted in the space of the standard normal probability distribution are assumed to represent mean daily temperatures. If they do not fall below the curve, the algorithm will assume that it has performed an unsuccessful simulation and will continue to the next pair of values.

3.3.2 Simulating Snowfall and Rainfall

Based on climate normal data, snowpacks tend to accumulate in December and persist until March (Table 3.6). Thus, it seems logical to use the GAWSER equations to simulate snowpack data for these four months. A procedure similar to the mean daily temperature algorithm can be used to simulate snowfall and rainfall. Using data from Table 3.6, one can calculate the probability of rainfall exceeding 0.2, 5, 10, or 25 mm in the same manner as temperature probabilities were computed. These values can be used to create a probability of occurrence plot for each month (Figure 3.12). Logarithmic trendlines were added for each set of points with good fits. These trendlines are used to simulate rainfall in the same manner as mean daily temperature was simulated (Table 3.7). In this case, however, a point falling above the trendline is not considered a failure, it is assumed that rain did not fall on that day.

Table 3.7: Rainfall Probability Equations for December, January, February and March Where P is Probability of Occurrence and r is Rainfall Depth (mm)

Month	Logarithmic Trendline Equation
December	P = -0.0471Ln(r) + 0.1538
January	P = -0.0286Ln(r) + 0.0798
February	P = -0.0317Ln(r) + 0.0884
March	P = -0.055Ln(r) + 0.1646

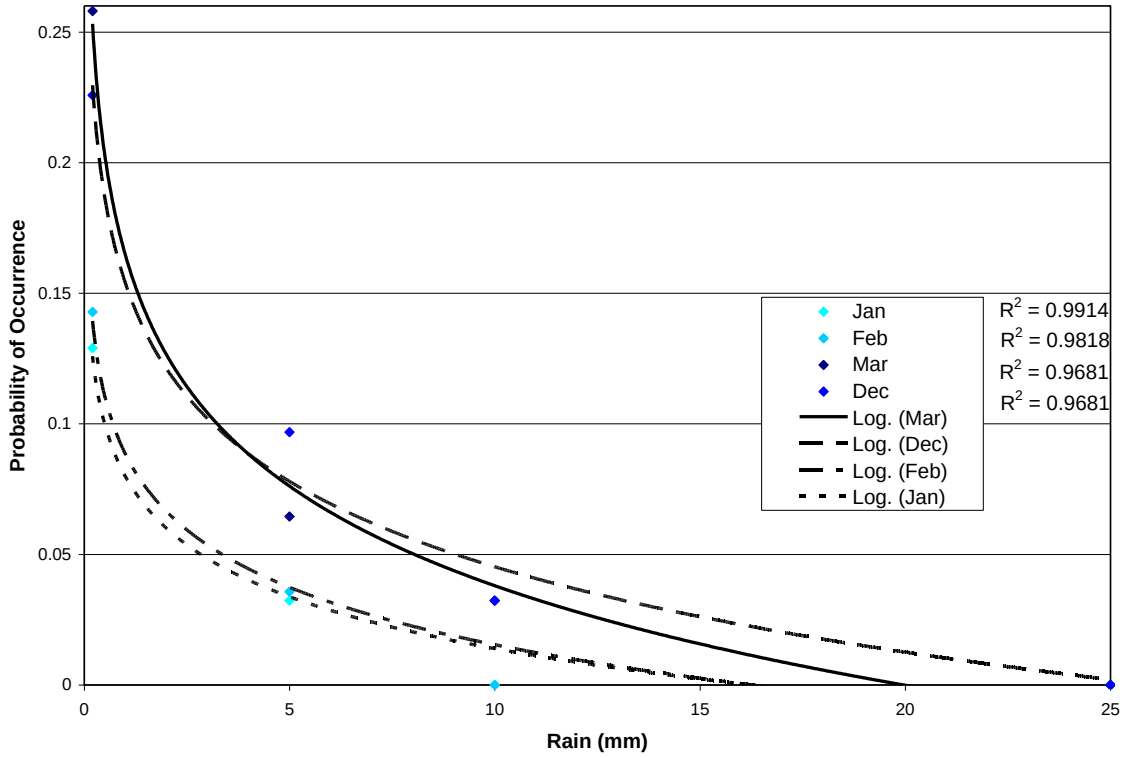

Figure 3.12: Probability of Occurrence of Rainfall for December, January, February and March

The same procedure was used to simulate snowfall (cm) (Figure 3.13 and Table 3.8).

3.4 Summary of Assumptions

Any model that is built to represent some physical process or phenomenon involves assumptions. Modellers must make these assumptions to simplify the task of building an algorithm or set of equations to represent nature. Assumptions are important to note since they have some impact on the accuracy of a model's predictions. There were five important assumptions made in this research.

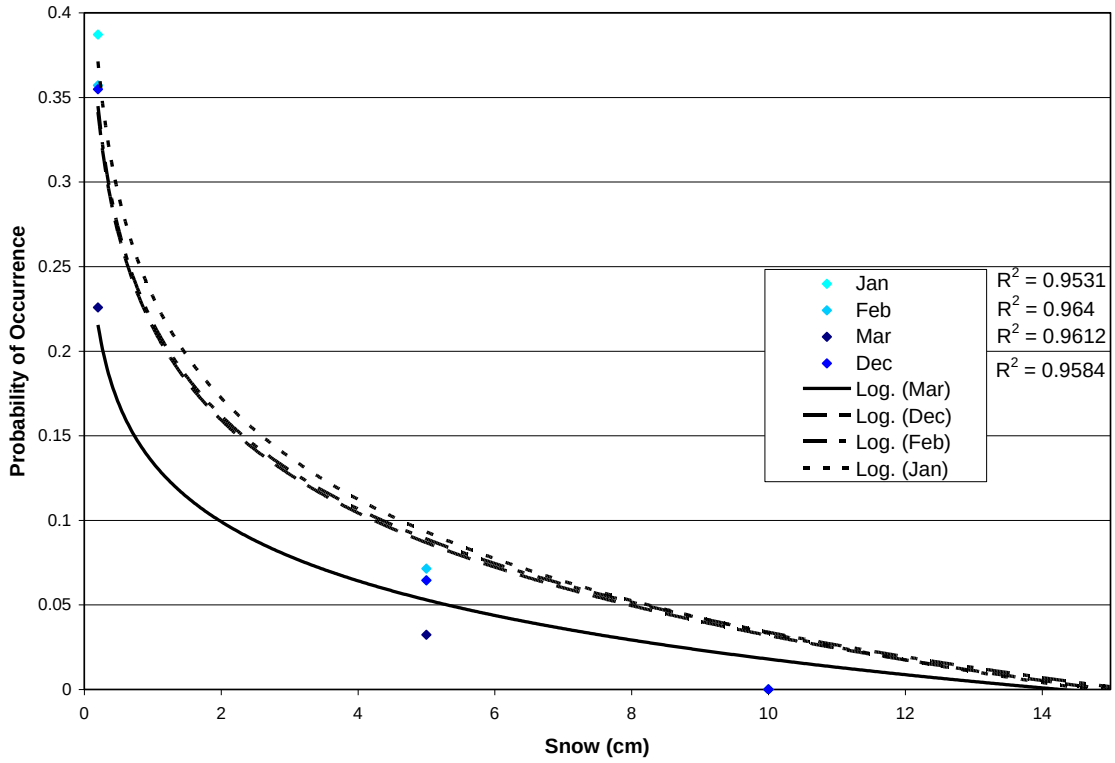

Figure 3.13: Probability of Occurrence for Snowfall in December, January, February and March

Table 3.8: Snowfall Probability Equations for December, January, February and March Where P is Probability of Occurrence and s is Snowfall Depth (cm)

Month	Logarithmic Trendline Equation
December	P = -0.0791Ln(s) + 0.2141
January	P = -0.0864Ln(s) + 0.2322
February	P = -0.0795Ln(s) + 0.2169
March	P = -0.0505Ln(s) + 0.1342

Three hydraulic radii were used to estimate travel times for channel flow. These radii represent respectively, the upper tributaries, the east and west branches of Duffins Creek and the main branch of Duffins Creek. It is assumed that the hydraulic radius is the same for any given cross-section in these three classes. In reality, channel geometry is complex and is influenced by many factors. The true hydraulic radius may in fact be

highly variable between different cross-sections of the same reach. This assumption is comparatively the most important since it influences both travel time (Equation 7) and flood stages.

A limitation related to the scope of this study was that field data could not be collected to verify some assumptions. One of these was the assumption that stream channels in the Duffins Creek watershed are half-pipe shaped. Several other channel shapes are possible including a V-shape, square trench shape or a smaller fraction of a pipe (i.e. ¼, ⅛, etc.). However, without field observations, it is fair to say that, initially, any one of these assumptions is as valid as the next. Through an extensive calibration procedure, an optimum channel shape could be chosen but such a procedure is out of the scope of this project.

It is also assumed that Manning's Roughness Coefficients for both stream channels and hydrologic units are essentially uniform. Based on orthophotographs (Triathlon Mapping Corporation, 1995), it was estimated that the majority of the watershed channels were fairly clean and relatively straight. Manning's Roughness Coefficient was chosen based on this estimation. However, it is likely variable in space for both stream channels and land units.

To calculate travel times, it was assumed that all runoff enters a stream channel at the outlet of the sub-basin where it was initiated. This is a simplification of reality, where runoff would enter the stream channel at many different places in each sub-basin. The

assumption was made for computational efficiency, but it had an impact on travel time accuracy.

Finally, rainfall inputs that are used to simulate runoff are assumed to be evenly distributed over the catchment. A real rainstorm might fall unevenly and might not cover the whole watershed area. It should also be noted that rainfall intensities for the design storms used to test this model are recorded in 15-minute intervals.

To assess the numerical impact of each of these assumptions on flood discharge and travel times a comprehensive calibration process would be required in which different scenarios would be run and compared. Comparison between the results of different test scenarios and control values would reflect on the validity of different assumptions. A comprehensive calibration process that would test all model assumptions is out of the scope of the current project given the time required to produce such a watershed model.

Chapter 4: Results and Discussion

4.1 GAWSER

4.1.1 Calibration of Snowfall and Rainfall Depths

Initial accuracy estimates for weather simulations revealed a problem with respect to snowfall and rainfall depth predictions. Originally, random probability data were constrained so that the highest value was 1 and the lowest was 0. In practice, this resulted in extreme underestimation of snowfall and rainfall depths. This problem was solved by reducing the spread of random probability values so that the maximum value was approximately equal to the highest solution of the corresponding logarithmic equations (Tables 3.7 and 3.8). In theory this solution corresponds to the probability (P) of the smallest snowfall (s) or rainfall that agrees with the original data (for snowfall in January as an example):

$$P = -0.0864\text{Ln}(s) + 0.2322; \text{ as s approaches } 0 \quad (29)$$

In practice, P was estimated in consecutive trials until a suitable result was obtained. Estimations were not undertaken beyond two decimal places because this would have been a time consuming process and small variations in P did not have a large impact on the accuracy of the simulations. Reducing the range of random probability data resulted in much improved accuracies for estimates of snowfall and rainfall depth.

4.1.2 Weather Simulation

Simulations of mean daily temperature using an algorithm based on random data were validated by comparison with climate normal data collected at Pearson International Airport (The Weather Network, 2003). Five different simulations were generated by varying the algorithm's seed. Changing the seed essentially changes the random values that are used to drive the algorithm. The seed itself is a value that determines where in the set of random values the algorithm will begin the simulation. It has minimum and maximum values of 1 and 10 respectively. Comparison of these simulations with climate normal values for December, January, February, and March revealed that no errors larger than 1°C were obtained (Table 4.1). The average error for all simulations is 0.55°C.

Table 4.1: Comparison of Average Mean Daily Temperatures (°C), Simulated and Gauge Data

Month	Mean Gauge Value	Simulation 1 (seed = 1)	Simulation 2 (seed = 2)	Simulation 3 (seed = 5)	Simulation 4 (seed = 7)	Simulation 5 (Seed = 10)
Dec	- 3	-3	-3	-3	-3	-3
Jan	-6	-5	-5	-5	-5	-5
Feb	-5	-5	-6	-6	-5	-6
Mar	0	1	0	1	1	0

These errors might have been lower if more temperature data were available. For example, the number of days less than or equal to 0°C could have been expanded upon by including the same statistic for other temperatures. This could have helped to better define the normal curve for each month. In a project of greater scope, this could have been accomplished by accessing a large range of gauge data or possibly by conducting field experiments. For the purposes of this project, the error obtained is acceptable since

the GAWSER equations are not sensitive to small variations in temperature. For example, one can infer from the form of the equations that a discrepancy of 0.55°C should not produce a significant error in the amount of snowmelt (Equation 13).

Rainfall depth simulations were tested by comparing gauge data (The Weather Network, 2003) with simulated results (Tables 4.2, 4.3, 4.4 and 4.5). Again, five simulations were generated by altering the algorithm's seed. Errors were quantified by tabulating the number of error days (differences in days for each rainfall depth) for each simulation (Table 4.6). Average error days range from 5.8 to 2.8. The December average is highest, mainly because of a particularly poor performance during Simulation 1. This reflects the fact that, although the algorithm is driven by random numbers, there can occasionally be a large concentration of like values. In this case, the use of a particular seed (6) resulted in an unusually large concentration of small rainfall events. Since similar values were not recorded in any other month for any of the five simulations, it is likely that overall model accuracy was not negatively affected in a significant way. In fact, avoiding use of the sixth seed would eliminate the chance of this event recurring altogether. However, it is important to note that when random numbers are used there is a chance that values in the tails of the distribution will occasionally be obtained. It is not advisable to avoid these numbers since they fall into the natural distribution even though they are farther from the mean than most other simulations. Rather, it is recommended that the chance of obtaining these values be accepted rather than reducing the randomness of the algorithm.

Table 4.2: Comparison of Simulated and Gauge Rainfall Data Distributions in December

Rainfall (mm)	Days >=, Gauge	Days >=, Simulation 1 (seed = 6)	Days >=, Simulation 2 (seed = 4)	Days >=, Simulation 3 (seed = 9)	Days >=, Simulation 4 (seed = 2)	Days >=, Simulation 5 (seed = 5)
0.2	7	11	7	8	7	6
5	3	9	5	4	3	5
10	1	6	3	1	3	2

Table 4.3: Comparison of Simulated and Gauge Rainfall Data Distributions in January

Rainfall (mm)	Days >=, Gauge	Days >=, Simulation 1 (seed = 6)	Days >=, Simulation 2 (seed = 4)	Days >=, Simulation 3 (seed = 10)	Days >=, Simulation 4 (seed = 2)	Days >=, Simulation 5 (seed = 5)
0.2	4	0	4	1	3	4
5	1	0	1	0	1	2
10	0	0	0	0	1	2

Table 4.4: Comparison of Simulated and Gauge Rainfall Data Distributions in February

Rainfall (mm)	Days >=, Gauge	Days >=, Simulation 1 (seed = 6)	Days >=, Simulation 2 (seed = 4)	Days >=, Simulation 3 (seed = 10)	Days >=, Simulation 4 (seed = 2)	Days >=, Simulation 5 (seed = 5)
0.2	4	6	2	4	2	1
5	1	4	0	0	0	1
10	0	1	0	0	0	0

Table 4.5: Comparison of Simulated and Gauge Rainfall Data Distributions in March

Rainfall (mm)	Days >=, Gauge	Days >=, Simulation 1 (seed = 6)	Days >=, Simulation 2 (seed = 4)	Days >=, Simulation 3 (seed = 10)	Days >=, Simulation 4 (seed = 2)	Days >=, Simulation 5 (seed = 5)
0.2	8	5	7	4	10	6
5	2	2	3	0	4	1
10	1	0	1	0	0	0

Table 4.6: Error Days for Rainfall Simulation in December, January, February and March

Month	Simulation 1 (seed = 6)	Simulation 2 (seed = 4)	Simulation 3 (seed = 10)	Simulation 4 (seed = 2)	Simulation 5 (seed = 5)	Average
Dec	15	2	2	6	4	5.8
Jan	5	0	4	2	3	2.8
Feb	6	3	5	1	3	3.6
Mar	4	2	7	5	4	4.4

Validation of the snowfall depth simulations was performed by comparing gauge data and simulated data (Tables 4.7, 4.8, 4.9 and 4.10). The method was essentially the same as for simulation of rainfall depth. Tabulation of the number of error days for each month reveals that snowfall was not estimated as accurately as rainfall (Table 4.11). Average error day counts range from 11.6 to 5.2. Examination of error distributions (Tables 4.7, 4.8, 4.9 and 4.10) indicates that the primary cause of error was underestimation of the number of days where snowfall depth was between 0.2 and 5 cm. This suggests that the logarithmic trendline might have underestimated the probability of small snowfalls. Fortunately, these snowfalls should not have a large impact on snowpack depths estimated using the GAWSER equations because they do not contribute greatly to the snowpack depth.

Table 4.7: Comparison of Simulated and Gauge Snowfall Data Distributions in December

Snowfall (cm)	Days >=, Gauge	Days >=, Simulation 1 (seed = 2)	Days >=, Simulation 2 (seed = 8)	Days >=, Simulation 3 (seed = 1)	Days >=, Simulation 4 (seed = 5)	Days >=, Simulation 5 (seed = 6)
0.2	11	4	3	5	4	5
5	2	0	1	2	3	1
10	0	0	1	1	0	1

Table 4.8: Comparison of Simulated and Gauge Snowfall Data Distributions in January

Snowfall (cm)	Days >=, Gauge	Days >=, Simulation 1 (seed = 2)	Days >=, Simulation 2 (seed = 8)	Days >=, Simulation 3 (seed = 1)	Days >=, Simulation 4 (seed = 5)	Days >=, Simulation 5 (seed = 6)
0.2	12	3	4	1	1	3
5	2	0	0	0	0	0
10	0	0	0	0	0	0

Table 4.9: Comparison of Simulated and Gauge Snowfall Data Distributions in February

Snowfall (cm)	Days >=, Gauge	Days >=, Simulation 1 (seed = 2)	Days >=, Simulation 2 (seed = 8)	Days >=, Simulation 3 (seed = 1)	Days >=, Simulation 4 (seed = 5)	Days >=, Simulation 5 (seed = 6)
0.2	10	5	5	1	1	7
5	2	0	2	1	1	0
10	0	0	1	0	0	0

Table 4.10: Comparison of Simulated and Gauge Snowfall Data Distributions in March

Snowfall (cm)	Days >=, Gauge	Days >=, Simulation 1 (seed = 2)	Days >=, Simulation 2 (seed = 8)	Days >=, Simulation 3 (seed = 1)	Days >=, Simulation 4 (seed = 5)	Days >=, Simulation 5 (seed = 6)
0.2	7	6	3	3	0	6
5	1	5	0	0	0	3
10	0	0	0	0	0	0

Table 4.11: Error Days for Snowfall Simulation in December, January, February and March

Month	Simulation 1 (seed = 2)	Simulation 2 (seed = 8)	Simulation 3 (seed = 1)	Simulation 4 (seed = 5)	Simulation 5 (seed = 6)	Average
Dec	9	10	7	8	8	8.4
Jan	11	10	13	13	11	11.6
Feb	7	6	10	10	5	7.6
Mar	5	5	5	8	3	5.2

4.1.3 GAWSER Snowpack Estimation

The GAWSER equations were run using the most successful (Simulation 5) and least successful (Simulation 4) snowpack depth simulations to estimate their accuracy. Validation was performed using gauge data (The Weather Network, 2003) for December, January, February, and March. The GAWSER equations were run to the 15th day of each month for both scenarios (the 14th for February). The accuracy of the predicted snowpack depth was assessed by comparison with gauge data (Table 4.12). Climate normal data collected at Pearson International Airport (Table 3.6) reports the average number of days

in each month where snowpacks with depths of 1, 5, 10, and 20 cm were observed. Comparison with these values was used to validate the simulations. It is assumed that, if a reasonable number of days on average for a given month had a snowpack depth in the range of the simulated value then simulations are probably accurate.

Snowpack depths appear to have been overestimated, particularly in March. This is partly a result of error in snowfall simulations. However, it may also be inferred that snowmelt was not simulated effectively. This could have resulted from a melt factor that is too low. Variation of the algorithm's seed only had a significant impact on snowpack depth in December. Otherwise, all simulations fell within the ranges set in the original data (i.e. <=1 cm, 5 cm etc.). This indicates that the variance in simulated snowpack depth is probably acceptable for this project even if snowpacks were overestimated.

Table 4.12: Simulations of Snowpack Depth Using GAWSER Equations and Number of Days in Corresponding Month Where the Equivalent Depth Was Observed

Month	Simulated Snowpack Depth (cm)	Number of Days With Equivalent Snowpack (Table 3.5)
December Best Simulation	2.59	17
December Worst Simulation	16.97	4
January Best Simulation	11.59	10
January Worst Simulation	10.47	10
February Best Simulation	11.51	9
February Worst Simulation	10.62	9
March Best Simulation	10.98	4
March Worst Simulation	17.57	4

4.2 Accuracy Assessment of Stream Discharge Simulations

4.2.1 Model Calibration and Validation

Initial stream discharge simulations revealed several significant differences between the simulated values and control values. First, an apparent systematic error was present that caused simulated discharge to be approximately one order of magnitude larger than the control values. This was most likely due to the fact that input rainfall was treated as uniform over the 15-minute time intervals. It may have been more appropriate to use a dimensionless equivalent triangular unit hydrograph to represent the rainfall input over each interval (Mays, 2001). This would ensure a more realistic approximation of the behaviour of a rainfall event. In practice, it appeared that the error could be corrected for by dividing simulated discharges by 10. Given the scope of the project, this was the best available solution. However, the resulting values were still larger than the control values.

This second source of error is more likely due to the physical representation of the watershed. The elimination of sinks and the forcing of all flowpaths to end at the outlet could possibly result in overestimation of discharges for small rainfall events. During these events, sinks and depressions could store or attenuate some runoff, thus decreasing the magnitude of peak discharge. During large rainfall events, however, sinks fill quickly and the volume of overflow is approximately equal to inputs of new runoff. Thus, peak discharge is not significantly affected by sinks (Doan, 2000). Another possible contributing factor for this error is underestimation of the initial abstraction. The initial

abstraction refers to the amount of rainfall required for the initiation of runoff (Woodward et al., 2001). Woodward et al. (2001) reported that assumptions related to the initial abstraction in the original formulation of the Curve Number Method may not be appropriate. This could lead to peak runoff for small rainfall events that is 60% greater than it should be. Although the error observed here was not nearly this large, underestimation of the initial abstraction could still have been partly responsible for the observed error.

To make simulated discharges approximate those calculated using unit hydrograph theory, it was necessary to multiply them by some value (x) to account for storage. The value of x, for a 2-year rainfall was determined by dividing peak discharges from Visual OTTHYMO by simulated peak discharges for 5 of the control points. Point 3 was considered to be an outlier due to an unusually large discrepancy between control and simulated discharges and was not included in the calculation of x. The value of x was determined to be 0.4. Anomalous values at Control Point 3 are due to the fact that a relatively large area drains to this point that was not included in the original boundary defined by the TRCA (Figure 3.3).

Simulations for a 2-year storm were run and the results were compared with data produced using Visual OTTHYMO (Table 4.13). Since Visual OTTHYMO values were computed using the first four hours of each design storm, simulations were performed using the same rainfall values. Percent difference (%Difference) for peak discharge values was calculated using:

$$\%\text{Difference} = (PD_C - PD_S)/PD_C \quad (30)$$

where PD_C is peak discharge from the control sample and PD_S is simulated peak discharge. Although discharge values were altered, simulated peak discharge was generally close to the control values. Exceptions are Point 3, which is anomalous due to a discrepancy in boundary definition and Point 6, which exceeds the project goal for peak discharge by about 1 m^3/s. This is a relatively small error given that the goal of the project was to simulate peak discharge within 10 m^3/s of the control value and peak discharge at Point 6 is nearly 60 m^3/s. Hence, discharge simulations at Point 6 could probably still be considered acceptable. Estimates of time to peak exceeded the goals of this project for Points 2, 5 and 6. The difference is greatest for Points 5 and 6. This may be due to the effect of tillage upstream of these points. Since they drain large portions of the watershed, diversion by tillage would have the greatest impact on these points because much of the contributing runoff crosses the mid and upper reaches of the watershed where agriculture is the dominant land use.

Table 4.13: Simulations of Peak Discharge and Time to Peak for a 2-year Rainfall Event Compared with Visual OTTHYMO data (Control)

Control Point	Time to Peak, Simulated (hours)	Time to Peak, Control (hours)	Peak Discharge, Simulated (m^3/s)	Peak Discharge, Control (m^3/s)	% Error for Peak Discharge
1	10	9.25	4.2	5	16.0
2	9.5	11	12.0	8.1	48.1
3	7	6.25	14.9	2.9	413.8
4	8	9.5	22.8	19.7	15.7
5	6	9.5	30.0	32.6	8.0
6	7.75	10.08	57.4	68.5	16.2

Simulation of discharge using 5-year and 10-year rainfall events required new estimates of x. This may be because these rainfall events mobilized more water that was stored in depressions or ditches during a 2-year rainfall event. Kumar et al. (2002) reported that hydrograph time to peak and peak discharge are both sensitive to velocity of flow and the length of the highest order stream channel. Thus, it is also possible that the estimations of velocity used for this model were more appropriate for simulating large rainfall-based runoff events. The length of the highest order stream channel may also have reduced travel time. For 5-year and 10-year rainfall events, x was estimated as 0.65 and 0.82 respectively by dividing control values by simulated peak discharge. It seems that simulated discharge approaches control values as rainfall depths increase. This indicates that the model may be more adept at estimating discharge resulting from large rainfall events.

Simulations of discharge for 5-year and 10-year rainfall events were compared with values estimated using Visual OTTHYMO (Tables 4.14 and 4.15). Simulations of peak discharge for Points 1, 2, 4, and 5 met the goals of this project. For both rainfall events, the original simulations (no multiplier) were quite close to values estimated by Visual OTTHYMO for Control Points 5 and 6. Thus, application of a multiplier common to all points actually decreased the accuracy of simulated discharges for these points. However, it would be difficult to avoid applying such a common value since this would decrease the model's consistency.

Table 4.14: Simulations of Peak Discharge and Time to Peak for a 5-year Rainfall Event Compared with Visual OTTHYMO data (Control)

Control Point	Time to Peak, Simulated (hours)	Time to Peak, Control (hours)	Peak Discharge, Simulated (m^3/s)	Peak Discharge, Control (m^3/s)	% Error for Peak Discharge
1	10	9	6.76	7.94	14.9
2	9.5	11	19.5	13.26	47.0
3	7	5	24.2	5.32	354.9
4	8	9.75	37.1	31.38	18.2
5	6	9	48.7	53.67	9.3
6	7.75	9.58	93.3	108.86	14.3

Table 4.15: Simulations of Peak Discharge and Time to Peak for a 10-year Rainfall Event Compared with Visual OTTHYMO data (Control)

Control Point	Time to Peak, Simulated (hours)	Time to Peak, Control (hours)	Peak Discharge, Simulated (m^3/s)	Peak Discharge, Control (m^3/s)	% Error for Peak Discharge
1	10	9	8.5	10.02	15.2
2	9.5	11	24.6	16.96	45.0
3	7	5	30.5	7.47	308.3
4	8	9.75	46.9	39.64	18.3
5	6	8.75	61.4	68.17	9.9
6	7.75	9.58	117.7	137.39	14.3

4.2.2 Sources of Error

Although not all model goals were achieved, the method that was used may still hold promise if sources of error can be identified. Calibration based on assumed sources of error yielded positive results. A systematic error encountered during calculation of discharge was crudely accounted for by simple division. However a more appropriate correction, which could not be applied due to time constraints, could use a dimensionless equivalent triangular unit hydrograph to model rainfall inputs for each 15-minute interval (Mays, 2001). Using this approach, the peak rainfall for each 15-minute interval (q_p) would be determined using

$$q_p = Q/t_p(2/(1+t_r/t_p)) \quad (31)$$

where Q is the total rainfall input for each 15-minute interval, t_p is the time to peak rainfall and t_r is the time of recession of rainfall. In practice, both t_r and t_p would equal 7.5 minutes (half the 15-minute interval).

Errors in the calculation of travel time may be attributed partially to the attenuation of overland flow by tillage. Several studies noted that runoff tends to flow along tillage lines instead of downslope (Souchere et al., 1998, Takken et al., 2001). Takken et al. (2001) reported that topography-based models had higher slopes than tillage-based models. This surely had an impact on travel times of overland flow.

Based on values of x, it seems that there was significant storage, which is probably related to sinks, in the catchment that was not accounted for by the model. This may also be attributed to an error in the original formulation of the Curve Number Method (Woodward et al., 2001). The value of x was higher for lower rainfall depths, indicating that the model may be better suited to simulating large floods. It would be ideal if x could be described by some simple relationship. Three rainfall events are probably insufficient to develop such a relationship but one can hypothesize what it might look like (Figure 4.1). A good fit was obtained using a linear trend line to model the relationship between rainfall depth and x. It seems that the model would be most proficient in simulating a rainfall event with a depth of approximately 71.6 mm.

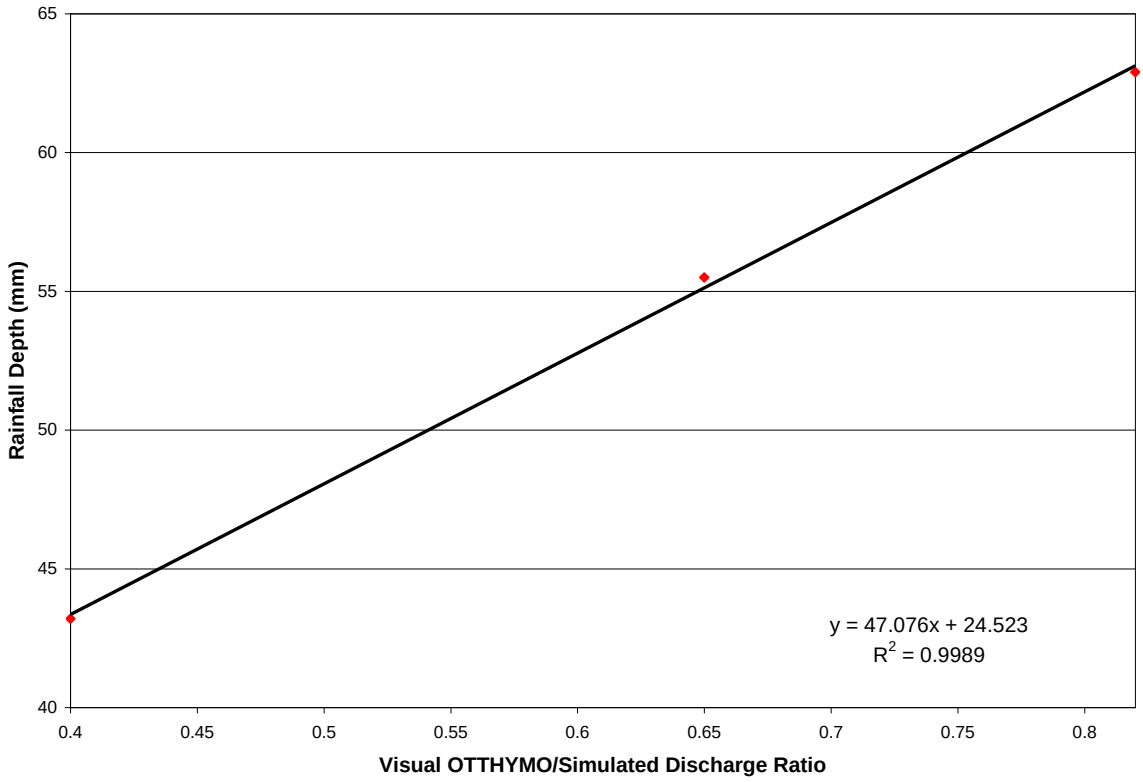

Figure 4.1: Relationship Between Rainfall Depth and Control/Simulated Discharge Ratio, Linear Trendline Fit

A final consideration is that some discrepancies may be due to the limitations of unit hydrograph theory. Advantages that the model may have over unit hydrograph theory stem from the fact that the latter does not simulate any of the physical properties responsible for runoff generation. It is scaled upward and downward based solely on rainfall depth.

In a project with greater scope, sources of error could potentially be identified through extensive model calibration. This would involve multiple simulations with different model parameters and perhaps different input data sets. For example, using an

unfilled DEM as an input could potentially reduce or even eliminate the need for a multiplier.

4.2.3 Runoff from Snowpack

Simulations of peak discharge were run assuming the presence of a snowpack on December 15th, January 15th, February 14th and March 15th. Results show that there was no noticeable effect on peak discharge (Table 4.16). Observation of individual values indicates that the snowpack contributed some additional runoff in nearly every case but not enough to significantly alter the peak discharge for any scenario. There would certainly be an effect on smaller rainfall events, particularly in March when melt and release of liquid water content from the pack were highest.

The effect of frozen ground could also be considered when simulating winter runoff. In theory, a frozen watershed should be nearly impermeable because pores are sealed by ice. Unfortunately, the Curve Number Method does not make allowances for the simulation of runoff from frozen ground. However, Fernhout and Kurtz (1998) suggested that multiplying S_{max} by 0.1 may be an appropriate alternative. Their idea was applied for December 15th at all control points (Table 4.17).

Table 4.16: Time to Peak and Peak Discharge Simulations With Snowpack for a 2-year Rainfall Event

Control Point and Month	Time to Peak (hours)	Peak Discharge (m^3/s)
Point 1, December	10	4.1
Point 2, December	9.5	12.0
Point 3, December	7	14.9
Point 4, December	8	22.8
Point 5, December	6	30.0
Point 6, December	7.75	57.4
Point 1, January	10	4.2
Point 2, January	9.5	12.0
Point 3, January	7	14.9
Point 4, January	8	22.8
Point 5, January	6	30.0
Point 6, January	7.75	57.4
Point 1, February	10	4.2
Point 2, February	9.5	12.0
Point 3, February	7	14.9
Point 4, February	8	22.8
Point 5, February	6	30.0
Point 6, February	7.75	57.4
Point 1, March	10	4.2
Point 2, March	9.5	12.0
Point 3, March	7	14.9
Point 4, March	8	22.8
Point 5, March	6	30.0
Point 6, March	7.75	57.4

Table 4.17: Time to Peak and Peak Discharge With Frozen Ground for a 2-year Rainfall Event

Control Point	Time to Peak (hours)	Peak Discharge (m^3/s)
1	9.5	12.7
2	9.5	32.1
3	7	38.1
4	8	66.8
5	5.75	80.4
6	7.5	163.7

The results seem to be somewhat high but unfortunately, no data are available to validate them (such as a hydrograph for a storm in winter or early spring).

4.3 Prediction of Inundated Areas

Inundated areas were predicted for 2-year, 5-year, and 10-year rainfall events using elevation values from the DEM (Figures 4.2 and 4.3). The resulting areas appear blocky and occasionally cross contour lines because they are limited by the DEM resolution. Significant inundation was only obtained at Points 4 and 6. This is because the stream channels at these points have fairly steep, but not near-vertical, slopes so the relatively small discharges resulting from the input rainfall can be visualized. For the other control points, verified discharges resulting from larger storms (i.e. 24-hour design storms) would be required to produce cartographically visible inundation given the DEM resolution. Risk areas extend for approximately 50 metres on each side of the bank near Point 4 and about 75 metres from each bank near Point 6. Since many more people live near Point 6 (Figure 4.3), one could infer that the risk to floodplain inhabitants is much greater than at Point 4. The risk appears to be especially great in the northern part of Figure 4.3.

All three rainfall events produced essentially the same inundated areas because the watershed is generally fairly flat. Stages (above bank elevation) were estimated for 2-year, 5-year and 10-year floods using simulated discharge values and cross-sections extrapolated from the DEM. 25-year, 50-year and 100-year stages were estimated using the same cross-sections and data from Visual OTTHYMO for comparison (Table 4.18).

The relatively small differences between stages are due to the fact that there is a wide flat plain over the banks of virtually any channel in the watershed. Channel velocity

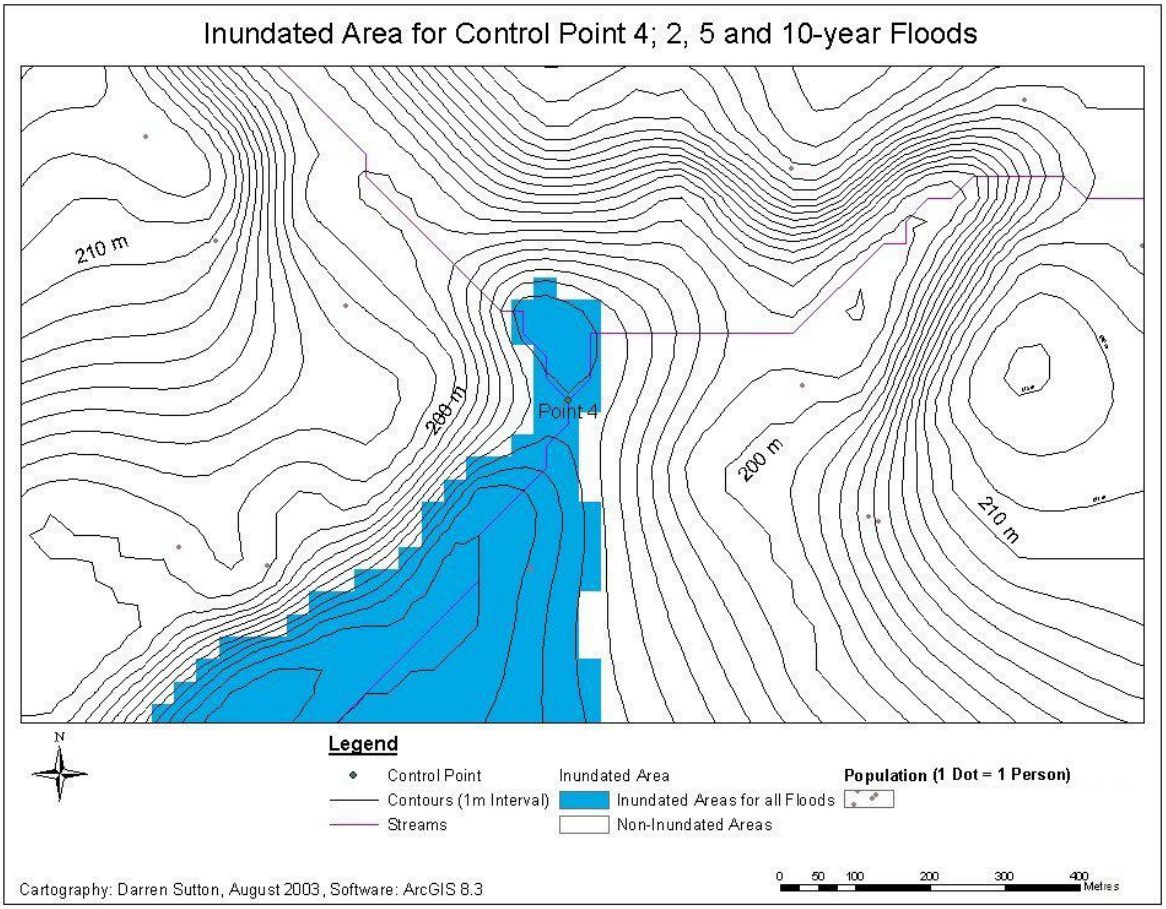

Figure 4.2 – Estimate of Inundated Area and Risk to Floodplain Inhabitants for Control Point 4

(as reported in TRCA data) increased noticeably between 2-year, 5-year, and 10-year rainfall events but remained fairly steady for 25-year and 50-year events. The increase in channel flow velocity partly accounts for the fact that stage remained relatively stable for 2-year, 5-year, and 10-year rainfall events. Stage values for these floods may be lower than predicted because simulated discharge values were used in conjunction with velocity

values from TRCA data. Combining these two data sets may account for the fact that stage did not greatly increase for 2-year, 5-year, and 10-year storms.

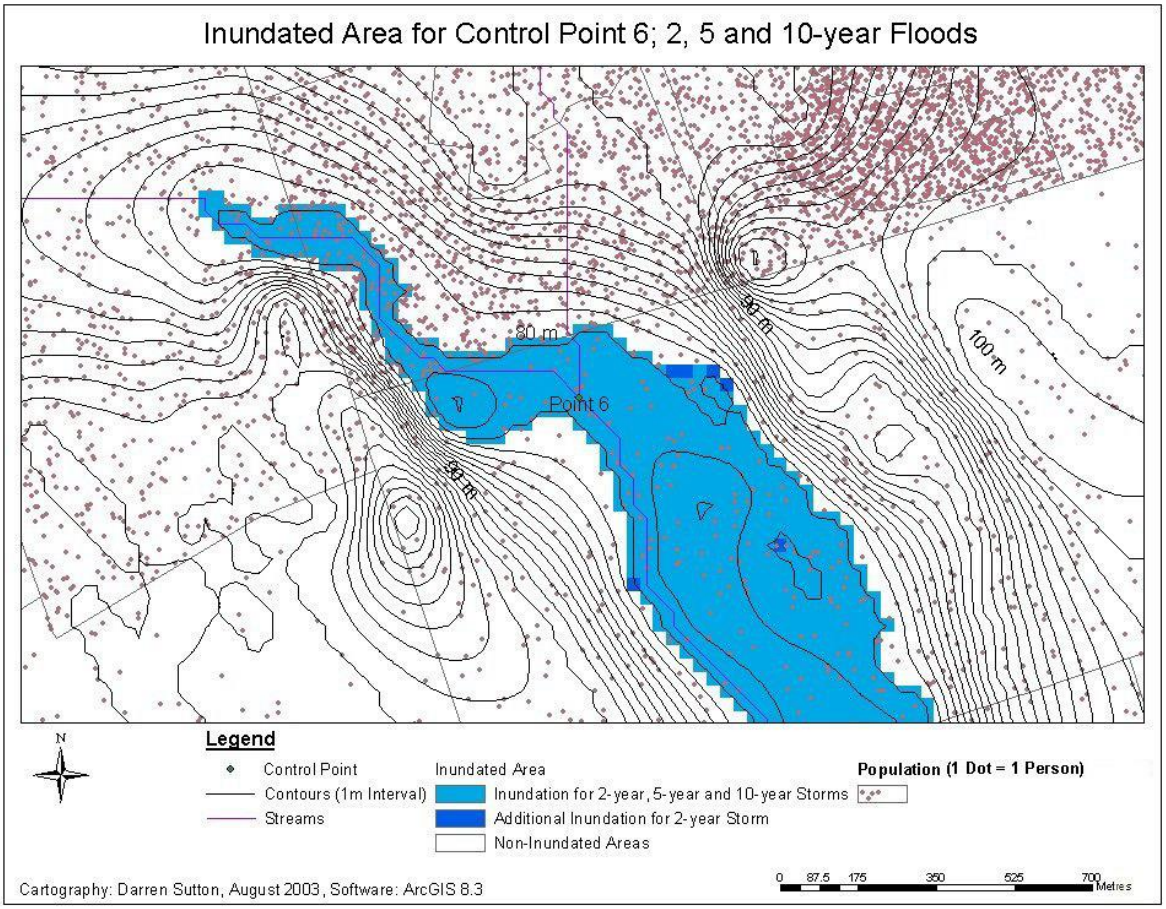

Figure 4.3 – Estimate of Inundated Area and Risk to Floodplain Inhabitants for Control Point 6

Table 4.18: Estimates of Stage (m) Above Bank Elevation for Control Points 4 and 6

Control Point	2-year Stage	5-year Stage	10-year Stage	25-year Stage	50-year Stage	100-year Stage
4	0.31	0.31	0.30	0.31	0.34	0.47
6	0.29	0.28	0.28	0.36	0.39	0.56

Peak discharge and time to peak data generated using Visual OTTHYMO used the first four hours of data from all design storms. This does not constitute the bulk of rainfall in any of the design storms. To illustrate the effect of a full design storm, stages were simulated for 2-year, 5-year, and 10-year design storms using the full 12 hours of rainfall data. Again, Control Points 4 and 6 were used (Table 4.19).

Table 4.19 – Estimates of Stage (m) Above Bank Elevation for Control Points 4 and 6 Using Full Rainfall Events

Control Point	2-year Stage	5-year Stage	10-year Stage
4	0.51	0.50	0.50
6	0.39	0.39	0.39

Chapter 5: Summary and Conclusions

This project used GIS tools and spatial data to create a flood-forecasting model for the Duffins Creek Watershed. The Curve Number Method was used to convert depths of rainfall into runoff using 15-minute time steps. Curve numbers are used to calculate the surface retention (S_{max}) for a given land unit. This parameter is important to the calculation of flood discharge since it determines how much rainfall is retained on the surface and in the soil before the inception of runoff. Curve numbers are determined based on the land cover, soil type, land use, and vegetation cover. Parcels of land with the same curve number are called hydrological response units.

Initial delineation of the watershed was accomplished using an extension for ArcView 3.2 called HEC-GeoHMS. This extension, designed by the United States Army Corps of Engineers, features a series of functions that divide a watershed into sub-basins and define stream networks. A Digital Elevation Model (DEM) of the Duffins Creek area with a 30-metre resolution was used as an input to HEC-GeoHMS. The Duffins Creek Watershed as delineated by HEC-GeoHMS is slightly larger than the Toronto and Region Conservation Authority's (TRCA) definition but stream networks defined by both sources are similar.

Hydrological response units were defined using ArcView Shapefiles of soil and land cover, digital orthophotographs, and a Landsat 7 satellite image. The TRCA supplied shapefiles containing land cover data and hydrological soil groups. Since these

files did not cover the entire watershed, additional data from the Ontario Ministry of Natural Resources (OMNR) and the Durham County Soil Survey were used to augment the TRCA files. Thus, two Shapefiles were obtained covering the watershed as defined by HEC-GeoHMS. Farming practices affect curve numbers so it was important to identify what kind of tillage is most common in the study area. Examination of digital orthophotographs revealed that most sloped agricultural terrain (i.e. next to a stream channels) showed evidence of contour tillage. Curve numbers for some land uses also depend on the amount of vegetation cover. The Leaf Area Index (LAI) was used as an indicator of this. Land cover, soil type, and LAI data sets were overlain to obtain a map of hydrological response units.

A set of points corresponding to the DEM cells was used to assign curve numbers to each point based on spatial association with hydrological response units. The travel time from each point to the watershed outlet was calculated for three phases of flow. It was assumed that sheet flow occurred for 92 meters from the beginning of flow. After the cessation of sheet flow, shallow concentrated flow persisted until runoff reached a stream channel. Upon entering a channel, runoff flowed as open channel flow to the outlet. A tally of travel times was computed for the outlet of each sub-basin and was further sub-divided by curve number. Thus, the amount of runoff arriving at any sub-basin outlet is obtained by multiplying the number of contributing points for the appropriate time step by the runoff depth obtained using the Curve Number Method.

The model was tested using 2-year, 5-year, and 10-year design storms obtained from the TRCA. Simulated peak discharge and time to peak were compared with corresponding values obtained via another model (Visual OTTHYMO) for six control points. Initial results were in error by a significant margin. A systematic error was diagnosed which caused simulated values to be greater than control values by approximately one order of magnitude. This was corrected by dividing the model results by 10. The performance of the model was improved with this correction but a more appropriate method would be to use an equivalent triangular dimensionless unit hydrograph. In the corrected model, performance was much better for large rainfall events than for small ones. A multiplier was introduced to modify the model results based on the depth of rainfall. It is estimated that model performance would be ideal for a rainfall depth of approximately 71.6 mm, which corresponds to a rainfall event that occurs approximately once per year. Application of an exponential curve to the design storms used in this research suggests that rainfalls of this depth probably occur several times in a year. For comparison, 2-year, 5-year, and 10-year rainfall events have total depths of 172.8 mm, 222 mm, and 251.6 mm respectively. The optimum depth is larger than the rainfall depths that were used as inputs to Visual OTTHYMO, which were drawn from the first four hours of design storms.

Reducing discharge values using a multiplier was necessary to obtain a better performance for small rainfall events. This may be because during large rainfall events, nearly all runoff flows directly to the outlet. In contrast, sinks and depressions may play a significant role in attenuating runoff during small rainfall events. Additionally, the

original formulation of the Curve Number Method is somewhat inadequate in relation to initial abstraction, especially during small rainfall events (Woodward et al., 2001).

Snowfall, rainfall, and temperature were simulated using 30 years of climate normal data and were tested by comparison with 30-year average values. Temperature simulations were found to be very close to average values. Rainfall was better simulated than snowfall (which had some large errors). Snowpack depths simulated using the GAWSER equations were overestimated, but did not vary greatly when the snowfall algorithm seed was altered. Errors are attributed to the choice of melt factor and errors in snowfall simulation. Simulations of runoff through a snowpack were not significantly different from simulations with no snowpack. Runoff increased slightly due to release of snowpack liquid water but peak discharge was not altered significantly. The effect of frozen ground is not easily simulated using the Curve Number Method, and no data were available to validate the resulting peak discharges, which were significantly greater than all other model results.

Inundated areas for 2-year, 5-year, and 10-year rainfall events were mapped at Control Points 4 and 6. Comparatively, the greater risk to floodplain inhabitants is at Point 6 because population is greater in the vicinity of this point. Stages were estimated for discharges that were simulated using 2-year, 5-year, and 10-year rainfall events and for 25-year, 50-year, and 100-year events using data from Visual OTTHYMO. Channel flow velocities were obtained from the TRCA's data, which may have resulted in errors for 2-year, 5-year, and 10-year event-based stages.

Although the results of simulating peak discharge and travel time failed to meet some project goals, the methods used in this project could potentially be applied by organizations such as the TRCA. The TRCA in particular, could use some variation of this method to simulate discharge using GIS instead of another flood forecasting software package. Simulating rainfall, snowfall, and temperature using climate normal data is an effective method for generating various scenarios for floods. It can also be applied with widely used software such as Microsoft Excel or Corel Quattro Pro rather than investing in hydrological modelling software. Additionally, in watersheds where annual snowmelt leads to potentially dangerous floods, the GAWSER equations could be used to simulate these events. Simulating snowpack accumulation, then simulating the runoff caused by the melting of the snow pack could accomplish this. For winters with particularly heavy snowfall, probability values could be reduced to increase snowfall frequency. The runoff model itself simulates large rainfall-driven floods well, although performance could be improved by accounting for watershed storage, possibly using an unfilled DEM.

It may not be necessary to use every cell in a DEM to estimate travel times. A version of the model that is more spatially lumped could prove to be equally effective and easier to prepare. For example, travel times could be computed for a set of points that are randomly distributed across the watershed. This could facilitate the creation of a set of travel time contours. Areas falling between two sets of contours are assumed to have the same travel time as the contour line closest to the outlet. Contours could be chosen to conform to the desired model resolution (i.e. one hour). A map of curve numbers could then be subdivided based on travel time contours.

An extensive calibration and verification procedure is also recommended to select the best model parameters and help reduce model error. This would involve producing several models by varying input parameters such as hydraulic radius, threshold contributing area for streams and the length of duration of sheet flow. Also, river gauge data would be a better control sample for model validation than the output of a flood forecasting model such as Visual OTTHYMO. Given sufficient funds and time, gauge data could be collected to support rainfall, snowfall, temperature, and snowpack simulation. One possible source is a meteorological station at Stouffville which may have long-term records. The reason for using such data is that a more reliable framework for predicting rainfall, snowfall and temperature in the Duffins Creek watershed could be obtained using a long record collected in the catchment. Also, field observations could help to derive a melt factor that is more appropriate for the watershed.

The use of a finer resolution DEM could reduce some errors related to the location of floodlines, calculation of watershed slope, and delineation of sub-basin boundaries. However, considerations such as increased computer processing requirements and the elevated cost of finer resolution DEM data would need to be balanced with project goals.

It is recommended that further development of the method used in this project follow several guidelines:

1) account for surface storage by analysis of an unfilled DEM,
2) develop contours of travel times built from a map of randomly distributed points,

3) vary the driving parameters of GAWSER equations to predict different snowmelt-related flood scenarios

4) use a finer resolution DEM,

5) use different values for model parameters and compare to find the optimum values,

6) obtain local meteorological and stream gauge data from the watershed for validation and to improve snowpack simulations, and

7) modify rainfall input data using an equivalent triangular dimensionless unit hydrograph.

References

(all urls current as of September 2003)

Al-Sabhan, W., M. Mulligan and G.A. Blackburn. 2003. A real-time hydrological model for flood prediction using GIS and the WWW. *Computers, Environment and Urban Systems* 27, 1: 9-32

Anderson, M.L., Z.Q. Chen and M.L. Kavvas. 2002. Coupling HEC-HMS with Atmospheric Models for Prediction of Watershed Runoff. *Journal of Hydrologic Engineering*. 7, 4: 312-318

Ardron, J. 2000. *Grid2Point Avenue Script*. Living Oceans Society, BC

Arnold, J.G., J.R. Williams, A.D. Nicks and N.B. Sammons. 1990. *SWRRB: A Basin-Scale Simulation Model for Soil and Water Resources Management*. College Station, TX: Texas A&M University Press

Bates, P.D. and A.P.J. De Roo. 2000. A Simple Raster-Based Model for Flood Inundation Simulation. *Journal of Hydrology* 236: 54-77

Bates, P.D., M.S. Horritt, C.N. Smith and D. Mason. 1997. Integrating Remote Sensing Observations of Flood Hydrology and Hydraulic Modelling. *Hydrological Processes* 11: 1777-1795

Barry, D.A. and K. Bajracharya. 1995. On the Muskingum-Cunge Flood Routing Method. *Environment International*. 21, 5: 485-490

Bedient, P.B. and W.C. Huber. 2002. *Hydrology and Floodplain Analysis: 3rd Edition*. Upper Saddle River, NJ: Prentice Hall

Beven, K. 2001. TOPMODEL Web Page. www.es.lancs.ac.uk/hfdg/topmodel.html

Beven, K. and J. Freer. 2001. A Dynamic TOPMODEL. *Hydrological Processes* 15: 1993-2011

Beven, K. 1997. TOPMODEL: A Critique. *Hydrological Processes* 11: 1069-1085

Blazkova, S. and K. Beven. 1995. Flood Frequency Prediction for Data Limited Catchments in the Czech Republic Using a Stochastic Rainfall Model and TOPMODEL. *Journal of Hydrology* 195: 256-278

Blevens, K. 2003. Velocity-Slope Profile. http://water.me.vccs.edu/courses/CIV246/diagram1.htm

Brennan, P. and G. Smith. 1997. Wetted Perimeter-Definition. www.amflow.co.uk/wetperim.htm

Burt, J.E. and G.M. Barber. 1996. *Elementary Statistics for Geographers*. New York, NY: The Guilford Press

Carpenter, T.M., J.A. Sperfslage, K.P. Georgakakos, T. Sweeney and D.L. Fread. 1999. National Threshold Runoff Estimation Utilizing GIS in Support of Operational Flash Flood Warning Systems. *Journal of Hydrology* 224: 21-44

Chow, V.T., D.R. Maidment and L.W. Mays. 1988. *Applied Hydrology*. New York, NY: McGraw-Hill Inc

Coroza, O., D. Evans and I. Bishop. 1997. Enhancing Runoff Modelling with GIS. *Landscape and Urban Planning* 38: 13-23

Correia, F.N., F.C. Rego, M.G. Saraiva and I. Ramos. 1998. Coupling GIS with Hydrologic and Hydraulic Flood Modelling. *Water Resources Management* 12: 229-249

Daly, S.F., R. Davis, E. Ochs and T. Pangburn. 2000. An Approach to Spatially Distributed Snow Modelling of the Sacramento and San Joaquin Basins, California. *Hydrological Processes*. 14: 3257-3271

Daviau, J.L., K. Adamowski and G.G. Patry. 2000. Regional Flood Frequency Analysis Using GIS, L-moment and Geostatistical Methods. *Hydrological Processes* 14: 2731-2753

De Roo, A.P.J., C.G. Wesseling and W.P.A. Van Deursen. 1999. Physically based river basin modelling within a GIS: the LISFLOOD model. *Hydrological Processes* 3: 870-881

De Roo, A.P.J. 1998. Modelling runoff and sediment transport in catchments using GIS. *Hydrological Processes* 12: 905-922

DMTI Spatial. 2002. *30-metre Resolution Digital Elevation Model*. Markham, ON

Doan, J.H. 2000. *Geospatial Hydrologic Modelling Extension HEC-GeoHMS User Manual*. Davis, CA: US Army Corps of Engineers

Doherty, C. and G. Switzer. *Flood Forecasting (FFOR) Program Manual*. Toronto, Ont: Environmental Water Resources Group Ltd.

Dunne, T. and L.B. Leopold. 1978. *Water in Environmental Planning*. San Francisco: WH Freeman

Eaglin, R.D. 1996. *Manning's Kinematic Solution*. www.cee.engr.ucf.edu/classes/cwr4101/old/tr55-3.htm

Edwards, K. 2002. *Manning's n Coefficients for Open Channel Flow*. http://www.lmnoeng.com/manningn.htm

Environmental Modelling Systems. 2002. Watershed Modelling System (WMS) Overview. www.ems-i.com/WMS/wms.html

ESRI. 2003. ESRI Homepage. www.esri.com

ESRI. 2001. ArcGIS Hydro Data Model. Redlands, CA.

Fernhout, P.D. and C.F. Kurtz. 1998. Garden with Insight v1.0 Help: Hydrology-Surface Runoff-Runoff Volume. www.gardenwithinsight.com/help100/00000006.htm

Francini, M., J. Wendling, C. Obled and E. Todini. 1996. Physical Interpretation and Sensitivity Analysis of the TOPMODEL. *Journal of Hydrology* 175: 293-338

Garcia, M.J.L. and A.M. Camarasa. 1999. Use of geomorphological units to improve drainage network extraction from a DEM. *International Journal of Applied Earth Observation and Geoinformation*. 1, 3. 187-194

Guntner, A., S. Uhlenbrook, J. Seibert and C. Leibundgut. 1999. *Hydrological Processes* 13: 1603-1620

Gurnell, A.M. and D.R. Montgomery (eds.). *Hydrological Applications of GIS*. Chichester: John Wiley and Sons

Haahr, M. 1998. *True Random Number Service*. www.random.org

Hall, A.J. 1981. *Operational Hydrology Report No. 18: Flash Flood Forecasting*. Geneva: World Meteorological Organization

Hansen, N.C., S.C. Gupta and J.F. Moncrief. 2000. Snowmelt Runoff, Sediment and Phosphorous Losses Under Three Different Tillage Systems. *Soil and Tillage Research* 57: 93-100

Hinckley Jr., J.A. 1996. *Object-GAWSER: Object-Oriented Guelph All-Weather Storm-Event Runoff Model Phase 1: Training Manual*. Hanover, NH: US Army Cold Regions Research and Engineering Laboratory

Holko, L. and A. Lepisto. 1997. Modelling the Hydrological Behaviour of a Mountain Catchment Using TOPMODEL. *Journal of Hydrology* 196: 361-377

Horritt, M.S. and P.D. Bates. 2002. Evaluation of 1D and 2D Numerical Models for Predicting River Flood Inundation. *Journal of Hydrology* 268, 1-4: 87-99

Horritt, M.S. and P.D. Bates. 2001a. Predicting floodplain inundation: raster-based modelling versus the finite-element approach. *Hydrological Processes* 15: 825-842

Horrit, M.S. and P.D. Bates. 2001b. Effects of spatial resolution on a raster-based model of flood flow. *Journal of Hydrology* 253: 239-249

Hromadka II, T.V. and C.C. Yen. 1996. An integrated stormwater management/GIS software system. *Environmental Software* 11, 4: 209-219

Huang, B. and B. Jiang. 2002. AVTOP: A Full Integration of TOPMODEL into GIS. *Environmental Modelling and Software* 17: 261-268

Huber, W.C. and W. James. 2003. EPA Storm Water Management Model (SWMM), Versions 4.31 and 4.4. http://ccee.oregonstate.edu/swmm

Hwang, D., H.A. Karimi and D.W. Hyun. 1998. Uncertainty Analysis of Environmental Models Within GIS Environments. *Computers and Geosciences* 24, 2: 119-130

Jain, S.K., R.D. Singh and S.M. Seth. 2000. Design Flood Estimation Using a GIS-Supported GIUH Approach. *Water Resources Management* 14: 369-376

Julien, P.Y., D.K. Molnar, B.E. Johnson and P.G. Combs. *Flood Forecasting Reaches New Potential*. www.agu.org/eos_elec

Karimi, H.A. and B.H. Houston. 1996. Evaluating Strategies for Integrating Environmental Models with GIS: Current Trends and Future Needs. *Computers, Environment and Urban Systems* 20, 6: 413-425

Karssenberg, D. 2002. The value of environmental modelling languages for building distributed hydrological models. *Hydrological Processes* 16: 2751-2766

Keskin, M.E. and N. Agiralioglu. 1997. A Simplified Dynamic Model for Flood Routing in Rectangular Channels. *Journal of Hydrology* 202: 302-314

Kirkby, M.J. 1997. TOPMODEL: A Personal Overview. *Hydrological Processes* 11: 1087-1097

Knighton, D. 1998. *Fluvial Forms and Processes: A New Perspective*. New York, NY: Oxford University Press Inc.

Kumar, R., C. Chatterjee, A.K. Lohani, S. Kumar and R.D. Singh. 2002. Sensitivity Analysis of the GIUH-based Clark Model for a Catchment. *Water Resources Management* 16: 263-278

Kutchment, L.S. and A.N. Gelfan. 1996. The Determination of the Snowmelt Rate and the Meltwater Outflow from a Snowpack for Modelling River Runoff Generation. *Journal of Hydrology* 179: 23-36

Lacroix, M.P., L.W. Martz, G.W. Kite, and J. Garbrecht. 2002. Using Digital Terrain Analysis Modelling Techniques for the Parameterization of a Hydrologic Model. *Environmental Modelling and Software*. 17, 2: 125-134

Lamb, R., K. Beven and S. Myrabo. 1997. Discharge and Water Table Predictions Using a Generalized TOPMODEL Formulation. *Hydrological Processes* 11: 1145-1167

Lamoureux, S.F. 2001. Geography 308: Watershed Hydrology Course Notes. Kingston, Ont: Queens University

Leavesley, G.H., S.L. Markstrom, P.J. Restrepo and R.J. Viger. 2002. A modular approach to addressing model design, scale and parameter estimation issues in distributed hydrological modelling. *Hydrological Processes* 16: 173-187

Lillesand, T. and R. Kiefer. 2000. *Remote Sensing and Image Interpretation*. New York, NY: Wiley and Sons

Mack, M.J. 1995. HER-Hydrologic Evaluation of Runoff: The Soil Conservation Service Curve Number Technique as an Interactive Computer Model. *Computers and Geosciences* 21, 8: 929-935

Magagi, R. and M. Bernier. 2003. Optimal Conditions for Wet Snow Detection Using RADARSAT SAR Data. *Remote Sensing of Environment* 84: 221-233

Mailhot, A., A.N. Rousseau, S. Massicotte, J. Dupont and J.P. Villeneuve. 1997. A Watershed-Based System for the Integrated Management of Surface Water Quality: the GIBSI System. *Water Science and Technology* 36, 5: 381-387

Markstrom, S. 2000. Modular Modelling System (MMS): A Modelling Framework for Multidisciplinary Research and Operational Applications. wwwbrr.cr.usgs.gov/mms/

Martin, P. 1999. Reducing flood risk from sediment-laden agricultural runoff using intercrop management techniques in northern France. *Soil and Tillage Research* 52, 3-4: 233-245

Martz, L.W. and J. Garbrecht. 1998. The treatment of flat areas and depressions in automated drainage analysis of raster digital elevation models. *Hydrological Processes* 12: 843-855

Mays, L.W. 2001. *Water Resources Engineering: 1st Edition*. New York, NY: Wiley and Sons

McKinney, D.C. and X.Cai. 2002. Linking GIS and water resources management models: an object-oriented method. *Environmental Modelling and Software* 17: 413-425

McLin, S.G., E.P. Springer and L.J. Lane. 2001. Predicting Floodplain Boundary Changes Following the Cerro Grande Wildfire. *Hydrological Processes* 15: 2967-2980

Melesse, A.M. and S.F. Shih. 2002. Spatially distributed storm runoff depth estimation Using Landsat images and GIS. *Computers and Electronics in Agriculture* 37, 1-3: 173-183

Mizanur-Rashid, R.S.M. and M.H. Chaudhry. 1995. Flood Routing in Channels with Floodplains. *Journal of Hydrology* 171: 75-91

Mockus, V. 1964. *National Engineering Handbook, Section 4: Hydrology*. ftp://ftp.wcc.nrcs.usda.gov/downloads/hydrology_hydraulics/neh630/

Molicova H., M. Grimaldi, M. Bonell and P. Hubert. 1997. Using TOPMODEL Towards Identifying and Modelling the Hydrological Patterns Within a Headwater, Humid, Tropical Catchment. *Hydrological Processes* 11: 1169-1196

Ontario Ministry of Natural Resources. 1998. *Ontario Land Cover Database*. Peterborough, ON: Ontario Ministry of Natural Resources

Osterkamp, W.R. and J.M. Friedman. 2002. The disparity between extreme rainfall events and rare floods with emphasis on the semi-arid American West. *Hydrological Processes* 14: 2817-2829

Overton, D.E. and M.E. Meadows. 1976. *Stormwater Modelling*. New York, NY: Academic Press

Pomeroy, J.W., D.M. Gray, K.R. Shook, B. Toth, R.L.H. Essery, A. Pietroniro, and N. Hedstrom. 1998. An Evaluation of Snow Accumulation and Ablation Processes for Land Surface Modelling. *Hydrological Processes* 12: 2339-2367

Portman, F.T. 1997. Hydrological Runoff Modelling by the Use of Remote Sensing Data with Reference to the 1993-1994 and 1995 Floods in the River Rhine Catchment. *Hydrological Processes* 11: 1377-1392

Rousseau, A.N., A. Mailhot, R. Turcotte, M. Duchemin, C. Blanchette, M. Roux, N. Etong, J. Dupont and J.P. Villeneuve. 2000. GIBSI: An integrated modelling system prototype for river basin management. *Hydrobiologia* 422/423: 465-475

Sands, R. 1997. Waterways Experiment Station, Sava River Team. http://chl.wes.army.mil/research/projects/sava/

Schreider, S.Y., A.J. Jakeman, J. Gallant, and W.S. Merritt. 2002. Prediction of Monthly Discharge in Ungauged Catchments under Agricultural Land Use in the Upper Ping Basin, Northern Thailand. *Mathematics and Computers in Simulation* 59, 1-3: 19-33

Schreider, S.Y. and A.J. Jakeman. 2001. Streamflow modelling on a subdaily time-step in the Upper Murray Basin. *Mathematical and Computer Modelling* 33: 659-668

Schreider, S.Y., D.I. Smith and A.J. Jakeman. 2000. Climate Change Impacts on Urban Flooding. *Climatic Change* 47: 91-115

Schreider, S.Y., P.H. Whetton, A.J. Jakeman and A.B. Pitlock. 1997. Runoff Modelling for Snow-Affected Catchments in the Australian Alpine Region, Eastern Victoria. *Journal of Hydrology* 200: 1-23

Scurlock, P.M.O., G.P. Asner and S.T. Gower. 2001. *Worldwide Historical Estimates of Leaf Area Index, 1932-2000*. www.osti.gov/bridge

Semàdeni-Davies, A. 1997. Monthly snowmelt modelling for large-scale climate change studies using the degree day approach. *Ecological Modelling* 101: 303-323

Skidmore, A. (Ed.). 2002. *Environmental Modelling with GIS and Remote Sensing*. New York, NY: Taylor and Francis

Sherman, L.K. 1932. Streamflow from Rainfall by the Unit-Graph Method. *Engineering News* 108: 501-505

Shiiba, M., L. Xavier, and Y. Tachikawa. 2000. Real-Time Stage and Discharge Estimation by a Stochastic-Dynamic Flood Routing Model. *Hydrological Processes* 14: 481-495

Sinnakaudan, S.K., A.A. Ghani, M.S.S. Ahmad, and N.A. Zakaria. 2003. Flood Risk Mapping for Pari River Incorporating Sediment Transport. *Environmental Modelling and Software* 18, 2: 119-130

Souchere, V., D. King, J. Daroussin, F. Papy and A. Capillon. 1998. Effects of tillage on runoff directions: Consequences on runoff contributing area within agricultural catchments. *Journal of Hydrology* 206: 256-267

Statistics Canada. 1996. *Census of Canada*. Ottawa, ON: Minister of Industry

Sui, D.Z. and R.C. Maggio. 1999. Integrating GIS with Hydrological Modelling: Practices, Problems and Prospects. *Computers, Environment and Urban Systems* 23, 1: 33-51

Svetlichnyi, A.A., S.V. Plotnitskiy and O.Y. Stepovaya. 2003. Spatial distribution of soil moisture content within catchments and its modelling on the basis of topographic data. *Journal of Hydrology* 277: 50-60

Takken, I., V. Jetten, G. Govers, J. Nachtergaele and A. Steegen. 2001. The effect of tillage-induced roughness on runoff and erosion patterns. *Geomorphology* 37: 1-14

The Weather Network. 2003. *Weather Statistics at Ajax, Ontario*. www.theweathernetwork.ca/weather/stats/pages/C02017.htm?CAON0006

Toronto and Region Conservation Authority. 2003. TRCA Website. www.trca.on.ca

Toronto and Region Conservation Authority. 2002a. Flood Forecasts and Design Storms for Duffins Creek Watershed using Visual OTTHYMO. Toronto, Ont.

Toronto and Region Conservation Authority. 2002b. Duffins Creek State of the Watershed Report. Toronto, Ont: www.trca.on.ca/water_protection/strategies/duffins

Toronto and Region Conservation Authority. 2000. Land cover and soil hydrologic units in the Duffins Creek Watershed. Toronto, Ont.

Town of Ajax. 2003. *Town of Ajax Website*. www.townofajax.com

Town of Whitchurch-Stouffville. 2003. *Town of Whitchurch-Stouffville Website*. www.town.whitchurch-stouffville.on.ca

Triathlon Mapping Corporation. *Colour Digital Orthophoto Data Set of GTA/Golden Horseshoe*. Burnaby, BC

Tsihrintzis, V.A. and R. Hamid. 1998. Runoff quality prediction from small urban catchments using SWMM. *Hydrological Processes* 12: 311-329

Van der Linden, S. and M. Woo. 2003. Application of Hydrological Models with Increasing Complexity to Subarctic Catchments. *Journal of Hydrology* 270, 1-2: 145-157

Van der Linden, S. and M. Woo. 2003. Transferability of Hydrological Model Parameters Between Basins in Data-Sparse Areas, Subarctic Canada. *Journal of Hydrology* 270: 182-194

Van der Perk, M., P.A. Burrough and G. Voigt. 1998. GIS-based modelling to identify regions of Ukraine, Belarus and Russia affected by residues of the Chernobyl nuclear power plant accident. *Journal of Hazardous Materials* 61: 85-90

Van Duersen, W., C. Wesseling, P. Burrough and D.J. Karssenberg. 1995. PC Raster Environmental Software. www.pcraster.nl

Wania, F. 1997. Modelling the Fate of Non-Polar Organic Chemicals in an Ageing Snowpack. *Chemosphere* 35, 10: 2345-2363.

Watercom Engineering. 2002. *Description: Visual OTTHYMO*. www.watercom.ca/modelling_visualotthymo.htm

Webber, L.R., F.F. Morwick and N.R. Richards. 1946. *Soil Survey of Durham County: Report No.9 of the Ontario Soil Survey*. Guelph, ON: Experimental Farms Service, Dominion Department of Agriculture and the Ontario Agricultural College

White, L.W., B. Vieux, D. Armand, and F.X. LeDimet. 2003. Estimation of Optimal Parameters for a Surface Hydrology Model. *Advances in Water Resources* 26, 3: 337-348.

Wilby, R.L., L.E. Hay and G.H. Leavesley. 1999. A comparison of downscaled and raw GCM output: implications for climate change scenarios in the San Juan River Basin, Colorado. *Journal of Hydrology* 225: 67-91

Wise, S. Assessing the quality for hydrological applications of digital elevation models derived from contours. *Hydrological Processes* 14:1909-1929

Woodward, D.E., R.H. Hawkins, R. Jiang, A.T. Hjelmfelt Jr., J.A.V. Mullem, and Q.D. Quan. 2001. *Runoff Curve Number Method: Examination of the Initial Abstraction Ratio*. http://class.et.byu.edu/ce531/Papers/CNInitialAbstraction.pdf

Yin, Z. and T.H.L. Williams. 1997. Obtaining Spatial and Temporal Vegetation Data from Landsat MSS and AVHRR/NOAA Satellite Images for a Hydrologic Model. *Photogrammetric Engineering and Remote Sensing* 63, 1: 69-77

Zaghloul, N.A. and M.A. Abu Kiefa. 2001. Neural network solution of inverse parameters used in the sensitivity-calibration analyses of the SWMM model simulations. *Advances in Engineering Software* 32: 587-595